

## Interplay Between Wind-Driven Advection and Mixing of Salt and Dissolved Oxygen in a Microtidal Estuary

Jianxing Wang<sup>1</sup> , Johanna H. Rosman<sup>1</sup> , James L. Hench<sup>2</sup> , Nathan S. Hall<sup>1</sup> ,  
Anthony C. Whipple<sup>1</sup>, and Richard A. Luettich Jr.<sup>1</sup> 

<sup>1</sup>Institute of Marine Sciences, University of North Carolina at Chapel Hill, Morehead City, NC, USA, <sup>2</sup>Marine Laboratory, Nicholas School of the Environment, Duke University, Beaufort, NC, USA

### Key Points:

- In shallow estuaries with small tides, wind-driven currents and mixing interact to control stratification and bottom oxygen concentration
- For cross- and up-estuary wind stress, advection decreases stratification and turbulence is increased, leading to a well-mixed water column
- For down-estuary wind stress, the water column becomes stratified or well-mixed depending on the balance of advection and enhanced mixing

### Correspondence to:

J. Wang,  
jianxing@email.unc.edu

### Citation:

Wang, J., Rosman, J. H., Hench, J. L., Hall, N. S., Whipple, A. C., & Luettich, R. A., Jr. (2025). Interplay between wind-driven advection and mixing of salt and dissolved oxygen in a microtidal estuary. *Journal of Geophysical Research: Oceans*, 130, e2025JC022802. <https://doi.org/10.1029/2025JC022802>

Received 6 MAY 2025  
Accepted 28 MAY 2025

### Author Contributions:

**Conceptualization:** Jianxing Wang, Johanna H. Rosman, James L. Hench, Nathan S. Hall, Richard A. Luettich Jr.  
**Investigation:** Jianxing Wang, Johanna H. Rosman, James L. Hench, Anthony C. Whipple  
**Methodology:** Jianxing Wang, Johanna H. Rosman, James L. Hench, Nathan S. Hall, Anthony C. Whipple, Richard A. Luettich Jr.  
**Resources:** Johanna H. Rosman, James L. Hench, Richard A. Luettich Jr.  
**Writing – original draft:** Jianxing Wang  
**Writing – review & editing:** Johanna H. Rosman, James L. Hench, Nathan S. Hall, Anthony C. Whipple, Richard A. Luettich Jr.

**Abstract** Most work on how estuarine dynamics impact dissolved oxygen (DO) distributions has focused on tides, but in shallow estuaries with large fetch or small tides, wind can be the primary mixing agent and also drives advection. To investigate how these processes affect DO distributions, an observational study was conducted in the shallow, microtidal Neuse Estuary. Salinity, DO, and velocity profiles were measured at multiple positions along and across the estuary over a 6-month period. A one-dimensional model (General Ocean Turbulence Model) provided additional insight into the response of salinity and DO to wind. Salinity and oxygen conservation equation terms were calculated from observations and simulations. Cross-estuary wind drove lateral circulation and tilted the isohalines, reducing stratification; lateral advection and enhanced mixing reduced vertical gradients and increased the bottom DO. Down-estuary wind tended to increase the exchange flow and stratification, but concurrently the surface wind-mixed layer deepened over time. The balance of these processes determined if the water column became fully mixed or remained stratified, and the depth of the pycnocline and oxycline. An expression for steady state surface layer thickness was derived by considering the competition between the horizontal and vertical buoyancy flux, and the predictions agreed well with observations and simulations. Up-estuary wind inhibited the exchange flow and the combination of advection and mixing homogenized the water column. While these patterns generally held for purely across- or along-channel wind, the response was often more complex as the wind vector varied in orientation and with time.

**Plain Language Summary** Dissolved oxygen (DO) is fundamental for marine ecosystems and can be depleted when benthic and water column consumption exceed replenishment via surface exchange with the atmosphere and vertical mixing. Estuaries with small tides often exhibit low DO near the bottom because turbulence is insufficient to mix the water column. In these estuaries, wind is important for driving currents and mixing, both of which affect vertical salinity gradients (stratification) and DO. We investigated wind effects on stratification and DO using measurements in the Neuse Estuary, which has very small tides, together with a simplified one-dimensional water column model. We found that wind blowing across the estuary or toward upstream mixes the water column and oxygenates bottom water. Wind blowing downstream generally enhances downstream current in the upper layer and upstream current in the lower layer which brings saltier ocean water into the estuary, increases stratification, and leads to low bottom DO. However, if the wind is strong enough it can generate enough turbulence to fully mix the water column and increase bottom DO. Further research is needed to understand how wind orientation and variability in time affect stratification and DO in estuaries.

## 1. Introduction

Dissolved oxygen (DO) is fundamental for marine ecosystems and constrains ocean productivity, biodiversity and biogeochemical cycles (Breitburg et al., 2018). DO has decreased in many coastal waters since the mid-1900s and hypoxia occurrences (DO < 2 mg/L, also termed dead zones) have doubled each decade (Diaz, 2001; Diaz & Rosenberg, 2008; Keeling et al., 2010). Anthropogenic nutrient loads and climate change are considered two major causes. A 43% increase in riverine nitrogen fluxes between 1970 and 2000 to coastal waters has resulted in eutrophication, dramatically increased primary production, harmful algal blooms, and depleted oxygen (Reed & Harrison, 2016). Although it is widely acknowledged that the increase of nutrient loads leads to an increase in the severity of hypoxia, correlating nutrient loads to interannual variations in hypoxic volume often fails to explain the majority of the variability (Hagy et al., 2004; Scully, 2010a). Also, substantial reductions in nutrient loads have been made along many coasts, but oxygen levels have not recovered as expected and have continued to decline (Lee & Lwiza, 2008; Riemann et al., 2015). Concurrent with increased nutrient inputs, a 2°C temperature

increase (which can also affect DO) was found in most dead zones by the end of the 20th century (Altieri & Gedan, 2015). A deeper understanding of the mechanisms of hypoxia is therefore needed.

Hypoxia occurs when biological consumption exceeds the rate of oxygen supplied by physical transport, air-sea fluxes and photosynthesis for sufficient periods of time (Breitburg et al., 2018). In estuarine and coastal areas, physical processes including vertical mixing and circulation patterns influence horizontal and vertical transport of DO. Stratification is considered a major cause of bottom hypoxia as it inhibits turbulent mixing and downward diffusion of DO from surface to bottom layers (Cui et al., 2019; Officer et al., 1984).

Wind forcing is known to affect estuarine circulation and stratification, especially in micro-tidal estuaries (Chen & Sanford, 2009; Li & Li, 2012; Scully et al., 2005; Xie & Li, 2018). It has long been recognized that wind stress is a source of energy that causes mixing and can reduce estuarine stratification (Simpson & Bowers, 1981; Simpson et al., 1991). Along-channel wind also plays an important role in determining the strength of the estuarine exchange flow and the corresponding increase or decrease in stratification (Scully et al., 2005). Chen and Sanford (2009) showed that up-estuary wind (wind directed toward up-estuary) tends to inhibit the exchange flow and decrease the stratification while down-estuary wind first increases then decreases the exchange flow and stratification. Such a transition results from the competition between wind straining and wind mixing. Wind straining is an increase or decrease in stratification caused by differential horizontal advection of salt in the upper and lower water column due to vertical shear in the wind-driven current. Wind stress also generates a turbulent surface boundary layer that grows downward with time and can erode stratification (Kato & Phillips, 1969). Under moderate down-estuary wind, wind straining dominates over wind mixing, causing stratification to increase; when the wind is strong, wind mixing exceeds wind straining and stratification is decreased (Chen & Sanford, 2009). Coogan and Dzwonkowski (2018) used long-term observations from Mobile Bay to investigate the along-channel wind effects on circulation and the results were consistent with Chen and Sanford (2009). Li and Li (2012) found from simulations that along-estuary wind could also drive lateral circulation due to the Coriolis effect, thereby tilting isopycnals and decreasing stratification.

Through its effects on the estuarine circulation and stratification, the wind can influence the DO dynamics and hypoxia at both timescales of individual events (hours to days) and seasons (Cui et al., 2019; Lee & Lwiza, 2008; Scully, 2010b, 2013). In Chesapeake Bay, all types of wind events decrease bottom hypoxic volume, but the extent differs with wind speed and direction (Scully, 2010b). In this large estuary (width ~30 km), lateral circulation driven by along-channel wind together with Coriolis, and enhanced vertical mixing due to the decreased stratification, are the dominant mechanisms for providing oxygen to bottom water. Although some wind directions increase stratification, which tends to decrease vertical mixing, lateral circulation provides oxygen to the bottom and is the dominant effect. The time-averaged effect of many individual wind events impacts seasonal variations in hypoxia. Scully (2013) found that in the Chesapeake Bay, the seasonal-average summer wind field results in more severe hypoxia compared to the winter wind field, exacerbating hypoxia that occurs due to high biological oxygen demand when water temperatures are warmer.

In smaller estuaries, processes are quite different; Coriolis forces are dynamically less important and DO distributions can respond more rapidly to changes in the wind field. For example, in the upper Neuse Estuary (width ~5 km), cross-channel wind drives lateral circulation and upwelling of low bottom DO and high salinity water at time scales of hours (Reynolds-Fleming & Luettich, 2004). It is expected that the effects of wind straining due to along-channel winds together with wind mixing that impact estuarine circulation and stratification (Chen & Sanford, 2009) also influence DO dynamics. However, the impacts of these processes on DO distributions are not well understood quantitatively.

In this study we investigated how the salinity and DO distributions in shallow microtidal estuaries respond to wind events with different wind speeds and directions over timescales of hours to days using field observations and idealized modeling. The Neuse Estuary is an ideal system in which to study these dynamics due to negligible tides, relatively strong winds and large fetch, and existing long time series of water quality measurements (Luettich et al., 2000; Paerl et al., 2010). Hypoxic and anoxic events have occurred frequently each summer in the Neuse Estuary for at least the past several decades (Buzzelli, Luettich, Powers, et al., 2002). Stronger stratification has been observed to exacerbate the hypoxia (Buzzelli, Luettich, Powers, et al., 2002), and cross-channel wind causes upwelling of low DO bottom water (Reynolds-Fleming & Luettich, 2004), but the dynamics causing these patterns have not been previously investigated. We qualitatively and quantitatively describe the impacts of wind direction and speed on salinity and DO distributions by analyzing data from events when wind is primarily cross-

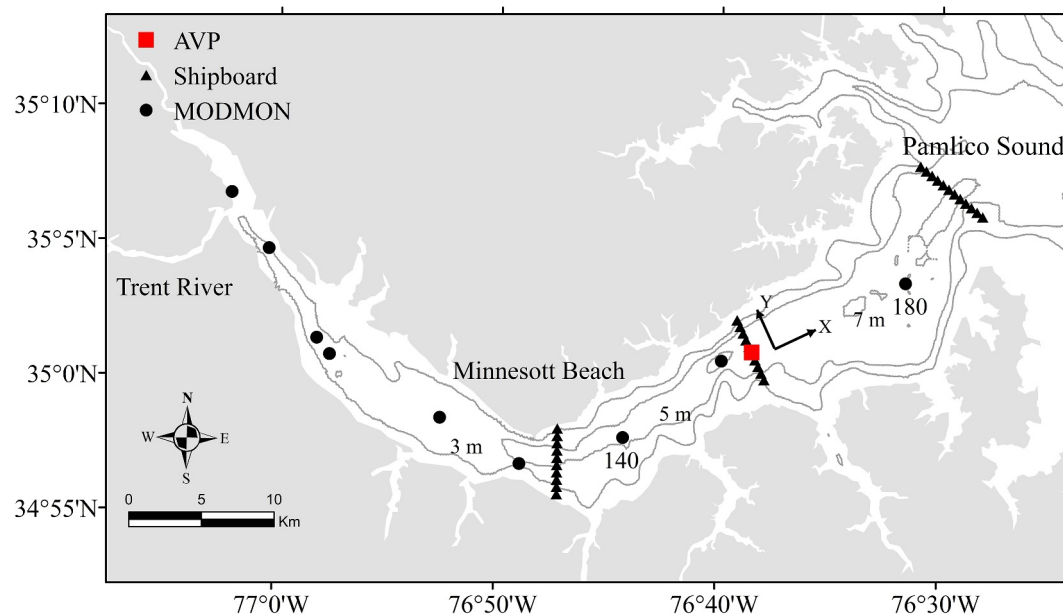


**Figure 1.** Study area, bathymetry, and observation sites in the Neuse Estuary. Red square is the central station where the Autonomous Vertical Profiler was located. The black triangles indicate shipboard acoustic Doppler current profiler/CTD stations. Black circles are ModMon stations, with stations 140 and 180 labeled.

estuary or along-estuary. Dominant mechanisms controlling the salinity and DO distributions under different wind conditions are assessed using salinity and DO budgets based on observational data and 1D model simulations. This study provides new insights into the impacts of wind with different speeds and directions on DO dynamics in estuaries where tides are small and the Coriolis effects are relatively unimportant.

## 2. Methods

### 2.1. Study Site

The Neuse Estuary is a 73 km-long estuary that connects with the Pamlico Sound. The estuary bends  $\sim 90^\circ$  at Minnesott Beach, which separates it into an upper part oriented roughly NW-SE and a lower part oriented roughly SW-NE (Figure 1). The Neuse is characterized as a shallow (average depth  $< 4$  m), microtidal (tidal range  $< 30$  cm) estuary (Luettich et al., 2000). Wind, therefore, is important for driving the mixing and circulation (Rizzo & Christian, 1996). The estuary varies from vertically well-mixed to highly stratified depending on the wind, and density stratification is controlled mainly by salinity gradients, which are dynamically much more significant than the temperature gradients (Whipple et al., 2006).

### 2.2. Field Measurements

Three sets of field observations were used in this study: (a) time series of velocity and water quality parameter profiles from moorings at a central site (site Autonomous Vertical Profiler (AVP) in Figure 1), (b) shipboard observations of velocity and water quality parameter profiles at stations along three cross-estuary transects, and (c) long-term shipboard observations of water quality parameters at stations along the estuary collected as part of the Neuse River Estuary Modeling and Monitoring (ModMon) program (Figure 1; Luettich et al., 2000).

The AVP site was at the center of the lower leg of the Neuse Estuary and was the focal site for the analysis. An AVP was four-point anchored in the middle of the estuary channel and measured profiles of salinity, temperature and DO from 16 May to 4 October 2016. The AVP is a floating platform with a robotic winch system that lowers a CTD/DO sensor (YSI, EXO2 Sonde) through the water column (Reynolds-Fleming et al., 2002; Whipple et al., 2006). The sonde was lowered at a constant rate of 0.01 m/s from the surface to 6 m depth at 30-min intervals. Only downcast data were used. An anemometer on the AVP platform measured the wind speed and direction 5 m above the water surface, also at 30-min intervals. A mooring was deployed adjacent to the AVP with

three CTD/DO sensors (SeaBird Electronics, SBE37-SMP-ODO) mounted 1.0, 2.9, and 4.7-m above the bottom. The more stable optical DO sensors on the mooring were used to correct for drift in AVP DO measurements in post-deployment processing. An upward-looking acoustic Doppler current profiler (ADCP, Teledyne RD Instruments 1.2-MHz Workhorse Monitor) mounted at the bottom (0.6 m above the seabed) adjacent to the AVP measured velocity profiles in 0.25-m vertical bins. The ADCP was programmed in fast ping mode (mode 12) with one ping every 6 s and 10 subpings per ping, and these data were averaged in 5-min time intervals for the analysis. A Nortek Aquadopp-HR 2 MHz profiler was deployed downward looking 1.7 m above the bottom for a 2-week period and measured near-bottom velocity profiles.

To measure the across-channel structure of salinity, DO and velocity, shipboard measurements were made along transects at the mouth, middle of the lower Neuse, and bend (Figure 1). There were 10–12 equally spaced stations (500 m apart) along each transect. Shipboard measurements were made on the 9-m R/V *Parker*. All three transects were collected quasi-synoptically (centered around noon) on eight cruises during the period the AVP and moorings were deployed (8 and 20 June, 5 and 18 July, 3 and 16 August, 7 and 19 September 2016). At each station, velocity profiles were measured with a boom-mounted ADCP (Teledyne RD Instruments 1.2 MHz Workhorse Monitor) (Hench et al., 2000) using 0.25-m bins for 6 minutes in mode 1 with 1 Hz ping rate. The vessel was nearly stationary while profiling, but the remaining motion was removed via ADCP bottom-track. Salinity, temperature and DO profiles were obtained from CTD casts (Seabird Electronics, SBE19plus V2) made at each station with a sampling rate of 4 Hz and averaged in 10 cm bins.

Vertical profiles of CTD/DO data were collected at a set of stations along the main axis of the Neuse biweekly as part of the long-term ModMon program.

### 2.3. Salinity and Oxygen Budget Calculations

Salinity and oxygen budgets were analyzed by calculating terms of the conservation equations from the field measurements. Vertical advection and horizontal mixing were assumed to be negligible compared with other terms. The conservation equation for salinity is

$$\frac{\partial S}{\partial t} = -u \frac{\partial S}{\partial x} - v \frac{\partial S}{\partial y} + \frac{\partial}{\partial z} \left( K_z \frac{\partial S}{\partial z} \right) \quad (1)$$

where  $S$  is the salinity,  $u$  and  $v$  are the along-channel and cross-channel velocities, and  $K_z$  is the vertical eddy diffusivity. The first two terms on the right are along- and cross-channel advection, and the third term represents vertical mixing.

The conservation equation for DO is

$$\frac{\partial \text{DO}}{\partial t} = -u \frac{\partial \text{DO}}{\partial x} - v \frac{\partial \text{DO}}{\partial y} + \frac{\partial}{\partial z} \left( K_z \frac{\partial \text{DO}}{\partial z} \right) + P \quad (2)$$

where we use “DO” to represent the concentration of DO and the first and second term on the right are the along-channel and cross-channel advection, the third term is the vertical mixing and the fourth term represents production and respiration by phytoplankton. The expression used for  $P$  is Jassby and Platt (1976)

$$P = PQ \frac{32}{12} C_{\text{chl}} \left( P_{\text{max}} \tanh \frac{\alpha I_z}{P_{\text{max}}} - R \right) \quad (3)$$

$$R = 0.1 P_{\text{max}} \quad (4)$$

where the  $PQ$  is the photosynthetic quotient for phytoplankton growing on ammonium (Oviatt et al., 1986; Smith et al., 2012),  $C_{\text{chl}}$  is the concentration of chlorophyll  $a$  and a typical value for the Neuse Estuary, derived from the ModMon data set, was used (Table 1).  $P_{\text{max}}$  is the average chlorophyll  $a$  specific light saturated photosynthetic rate and  $\alpha$  is the average slope of the light-limited region of the  $P$  versus irradiance relationship. Values for  $P_{\text{max}}$  and  $\alpha$  were gathered from previous measurements of photosynthesis versus irradiance on Neuse Estuary

**Table 1**  
Phytoplankton Production and Respiration Parameter Values Used in Equation 3–6

Parameters	Values
$PQ$	1.24
$C_{\text{chl}}$ (mg/L)	0.015
$P_{\text{max}}$ (mg <sub>carbon</sub> /mg <sub>chl</sub> /s)	0.0012
$\alpha$	0.0518
$K_d$ (1/m)	-1.27
$I_{\text{max}}$ (μmol/m <sup>2</sup> /s)	2,000

phytoplankton assemblages made by Buzzelli, Luettich, Paerl, et al. (2002).  $I_z$  is the irradiance at distance  $z$  from the water surface, where  $z$  is positive upwards, based on Beer's law:

$$I_z = I_o e^{K_d z} \quad (5)$$

where  $I_o$  is the incident irradiance:

$$I_o = \begin{cases} -I_{\text{max}} \cos 2 \pi t, & \cos 2 \pi t < 0 \\ 0, & \cos 2 \pi t \geq 0 \end{cases} \quad (6)$$

$t$  is time in days ( $t = 0$  is midnight).  $I_{\text{max}}$  is the maximum irradiance at the surface.  $K_d$  in Equation 5 is the extinction coefficient for photosynthetically active radiation calculated based on observations of light attenuation with depth from the ModMon data set.  $R$  is the respiration rate of the phytoplankton and it is set as 10% of  $P_{\text{max}}$  (Equation 4). The values of parameters from Equations 3 to 6 are shown in Table 1.

Every term in Equations 1 and 2 was calculated at the AVP station except the mixing term because  $K_z$  was not known. The along-estuary gradients,  $\frac{\partial S}{\partial x}$  and  $\frac{\partial DO}{\partial x}$ , were calculated based on the AVP and two adjacent ModMon stations (Station 140 and 180, Figure 1). The across-estuary gradients,  $\frac{\partial S}{\partial y}$  and  $\frac{\partial DO}{\partial y}$ , were calculated based on the AVP and two adjacent central transect shipboard stations (5 and 7). The horizontal velocity measured by the bottom-mounted ADCP was decomposed into along-channel ( $x$ ) and cross-channel ( $y$ ) components ( $u, v$ ). The major axis of the depth-averaged velocity from the 6-month data set was used to define the along-channel direction (with positive seaward; Figure 1).

#### 2.4. Idealized Simulations

Idealized simulations were used to investigate the role of turbulent mixing for the salinity and DO dynamics. The General Ocean Turbulence Model (GOTM) was used to simulate the evolution of velocity and salinity profiles, and turbulence properties under different wind conditions. GOTM is a 1-dimensional (vertical) model that solves the transport equations of momentum, salt and heat (Umlauf et al., 2005). It contains multiple well-tested turbulence models that are widely used (Ladwig et al., 2021; Lange & Burchard, 2019).

The model setup was based on the observational data, with a depth of 6.3 m and initial salinity and temperature profiles from 20 June. The vertical grid spacing was 0.1 m and the timestep was 0.01 s. The model was initialized with velocity, vertical eddy viscosity and diffusivity set to zero. The vertical eddy viscosity and diffusivity were calculated using the Mellor-Yamada 2.5 turbulence closure (Mellor & Yamada, 1982) with the stability function proposed by Schumann and Gerz (1995). The bottom hydrodynamic roughness ( $z_0$ ) was calculated from a log fit to velocity profiles measured with the downward-looking Aquadopp-HR current profiler at the AVP station. Model directions were defined such that  $x$ - and  $y$ -directions represent the along- and across-channel directions, respectively (Figure 1). Constant along-channel and lateral salinity gradients ( $\frac{\partial S}{\partial x}$ ,  $\frac{\partial S}{\partial y}$ ) from the data were used. The model was forced by winds (Table 2) in either the positive (toward down-estuary) or negative (toward up-estuary)  $x$  direction or in the  $y$  (cross-estuary) direction and a constant river inflow (0.01 m/s) in the  $x$  direction. River inflow velocity was estimated based on the average river discharge for the Neuse from USGS Station 02091814 divided by the cross-sectional area at the study site. Tides and the Coriolis parameter were set to zero. Wind stress was computed from the AVP met station measurements by first correcting for sensor height relative to a 10-m reference level using Blanton et al. (1989), and then using the wind speed dependent drag coefficients from Large and Pond (1981).

Down-, up-, and cross-estuary wind events were simulated to investigate wind effects on salinity and oxygen budgets. For down-estuary winds, simulations were run for three wind speeds (5, 7, 9 m/s) to investigate the implications for wind straining and wind mixing. For up and cross-channel winds, the wind speed was 5 m/s. For the along-channel wind cases, the cross-estuary salinity gradient  $\frac{\partial S}{\partial y}$  was set as zero. Each simulation was run for 60 hr starting from midnight, except for the 7 m/s down-estuary wind scenario which was run for 1 month to capture the final steady state dynamics. GOTM simulation parameters are summarized in Table 2.

**Table 2**  
General Ocean Turbulence Model Model Input Parameters for the Idealized 1D Simulations

Parameters	Values
Down-estuary wind (m/s)	5; 7; 9
Up-estuary wind (m/s)	5
Cross-channel wind (m/s)	5
$\frac{\partial S}{\partial x}$ (PSU/m)	$1.20 \times 10^{-4}$
$\frac{\partial S}{\partial y}$ (PSU/m)	$-1.05 \times 10^{-4}$
$\frac{\partial DO}{\partial x}$ ((mg/L)/m)	$1.68 \times 10^{-5}$
$\frac{\partial DO}{\partial y}$ ((mg/L)/m)	$3.51 \times 10^{-4}$
River inflow (m/s)	0.01
$z_0$ (m)	$6.8 \times 10^{-3}$
$C_d$	$1.14 \times 10^{-3}$
SOD ((mmol/m <sup>2</sup> )/d)	25

Velocity, temperature and eddy diffusivity profiles from GOTM output were used to compute the terms in the DO conservation equation. Along- and across-channel oxygen gradients ( $\frac{\partial DO}{\partial x}$ ;  $\frac{\partial DO}{\partial y}$ ) were set to constant values based on observations for simplification. The across-channel oxygen gradient ( $\frac{\partial DO}{\partial y}$ ) was set as zero for the along-channel wind events. The air-sea oxygen exchange was included as a flux boundary condition at the water surface. The expression for air-sea oxygen flux is Wanninkhof et al. (2009):

$$ASX = k k_o \Delta P_{O_2} \quad (7)$$

where  $k$  is the piston velocity and  $k_o$  is Henry's constant.  $\Delta P_{O_2}$  is the difference between the partial pressures of oxygen in the air and water. The expression for  $k$  is:

$$k = k_{600} \frac{S_c}{600}^{-0.5} \quad (8)$$

where the  $k_{600}$  is the piston velocity of CO<sub>2</sub> and the  $S_c$  is the Schmidt number for oxygen based on Wanninkhof et al. (2009). The sediment oxygen demand (SOD) was applied as a constant flux at the bottom boundary and was set to 25 mmol/(m<sup>2</sup> d) based on observations from previous studies (Luettich et al., 2000). The production and respiration term was calculated using Equation 3 with the values of parameters shown in Table 1. The conservation equation for DO (Equation 2) was solved using a forward differencing scheme.

### 3. Results

#### 3.1. Overview of Field Observations

During the 6-month observation period, stratification strength and bottom DO were qualitatively correlated (Figure 2). In June and September, the wind was mostly in the NE (toward north shore) and SW (toward south shore) directions (Figure 2a) and had both an along-channel and cross-channel component in the lower Neuse. During July and August, there was strong variability in wind speed and direction at diurnal frequencies due to the sea breeze. Stratification, expressed as salinity difference between surface and bottom ( $\Delta S$ ), generally correlated with the along-channel wind, increasing with down-estuary wind and decreasing with up-estuary wind. Bottom DO was inversely correlated with the along-channel wind and  $\Delta S$ , decreasing during down-estuary wind when the water column was more stratified and increasing during up-estuary wind when the water column was more mixed. Bottom DO was almost completely depleted (anoxic) in the observation area for about a month from 18 July to 28 August under the continuous moderate down-estuary wind condition and finally increased when the wind switched to the up-estuary direction for about 3 days after 28 August (Figure 2a).

Two days were selected from the 6-month data set to study the wind effects on the salinity and DO dynamics: 20 June to 21 June at noon and 19 September (Figures 3 and 4) because they contained events in which the wind was oriented in the along-channel and cross-channel directions for sufficient duration, and because all the data sets spanned these days. On 20 June, the wind blew south-eastward, cross-channel toward the south shore, during the first half of the day and switched to a north-eastward, down-channel direction during the latter half of 20 June into 21 June (Figure 3a). On 19 September, the wind blew north-westward, cross-channel toward the north shore, during the first half and turned to south-westward toward the up-channel direction during the latter half (Figure 4a).

On 20 June, when the wind had a significant cross-channel component during the first half of the day, significant lateral circulation was observed with a maximum speed of 0.2 m/s (Figures 3c and 5a). Considering a slice across the estuary and looking in the downstream direction, clockwise circulation developed and fresher surface water was advected to the south shore and saltier bottom water was advected to the north shore. The halocline, therefore, was tilted and stratification decreased. Bottom low DO water was also advected to the north shore (Figure 5c). As the down-estuary component of the wind increased in the second half of the day, the exchange flow strengthened

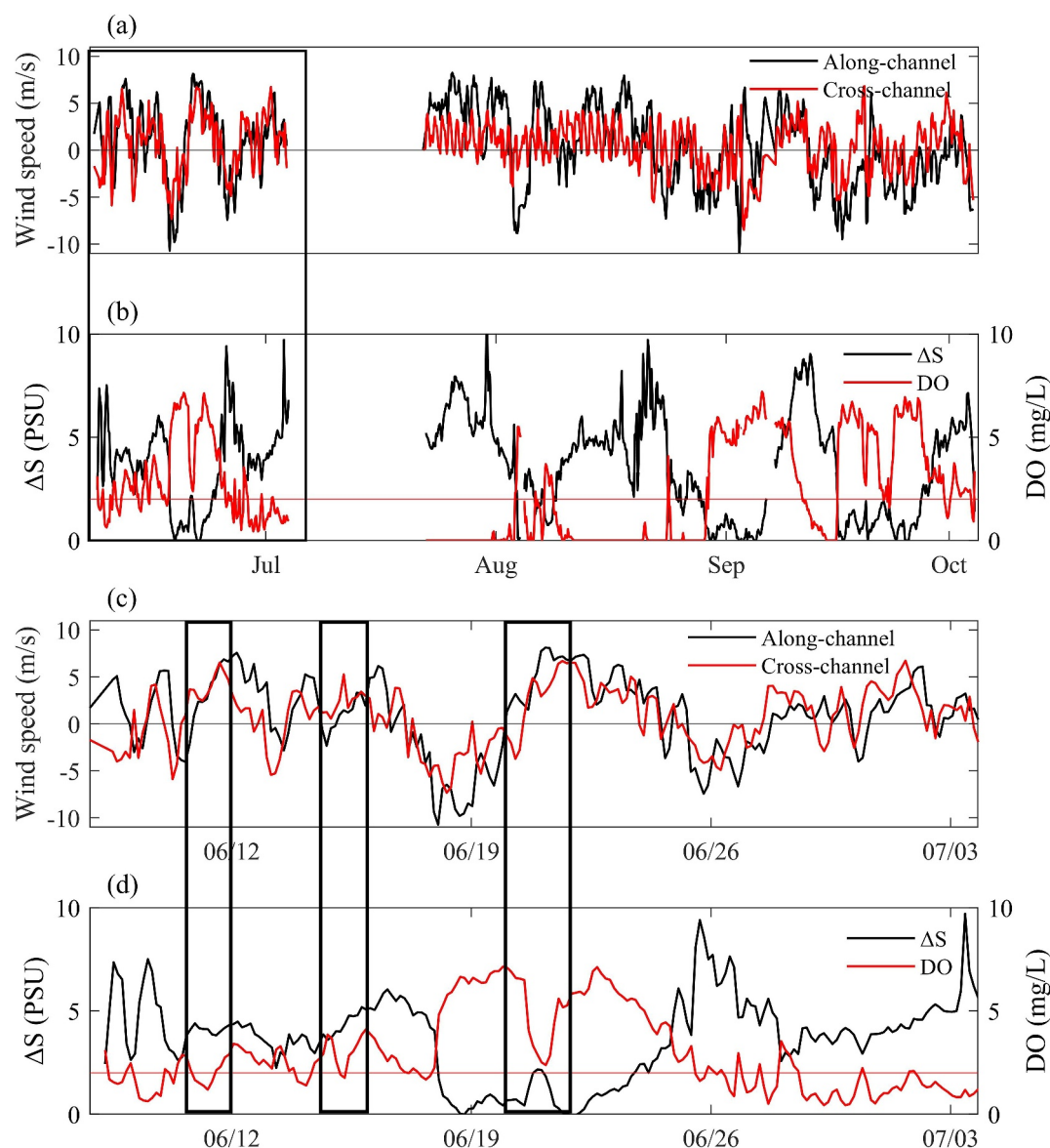


**Figure 2.** Time series of 3 hr-averaged along- and cross-channel wind components, salinity difference between surface and bottom 0.5 m ( $\Delta S$ ), and dissolved oxygen averaged over bottom 0.5 m. (a, b) Data during 8 June–4 October and (c, d) zoom of time period in the black box in (a) and (b). Positive along-channel wind is toward downstream and cross-channel wind is toward the north shore. The three black boxes in panels (c, d) are exceptions mentioned in Section 4.

and the surface outflow layer deepened (Figure 3b). The lateral circulation switched direction for a period of 2–3 hr after wind direction changed from cross-estuary to down-estuary, likely due to relaxation of sloped isopycnals, and then stopped (Figure 3c). High salinities were observed at the bottom, probably due to the combination of advection of high salinity water from the north side to the center channel by the lateral circulation, and the increased exchange flow (Figure 3d). DO concentrations in this layer were very low ( $DO < 2$  mg/L, Figure 3e). With the increase of the wind speed, the halocline deepened and finally disappeared at noon on 21 June at which time the water column was well-mixed. The roles of along-channel advection, lateral advection, and vertical mixing in controlling the salinity and DO distribution are assessed in Section 3.3. The low DO layer also decreased in thickness and disappeared when the water column became well-mixed. After midnight, the exchange flow began to decrease and disappeared in several hours, possibly due to barotropic (water surface slope) and baroclinic pressure gradients (isopycnal tilt) that balanced the wind stress.

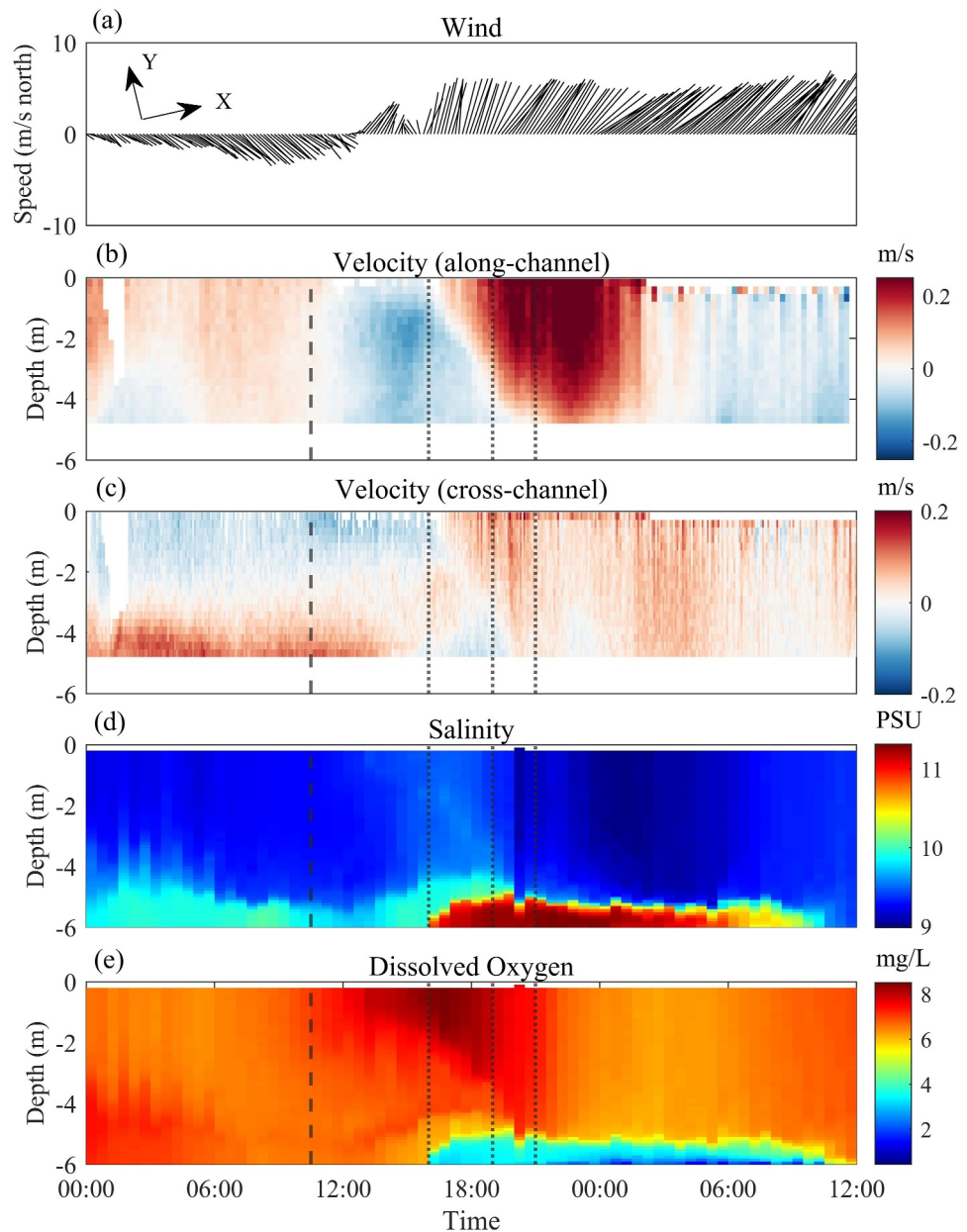


**Figure 3.** Time series of field observations at the Autonomous Vertical Profiler station on 20 and 21 June. (a) Wind velocity, (b) along-channel velocity, (c) cross-channel velocity, (d) salinity, and (e) dissolved oxygen. Positive along-channel is down-estuary and positive cross-channel is toward the north shore. The vertical black dashed line at 10:30 is the time selected for the budget calculations for the cross-channel wind case. The black dotted lines are the times (16:00, 19:00, 21:00) for the budget calculations for the down-estuary wind case.

On 19 September, the wind first blew toward the north shore (Figure 4a) resulting in counter-clockwise (when looking down-estuary) lateral circulation with maximum speed of about 0.2 m/s (Figure 4c). Surface fresher water was advected to the north shore and bottom saltier water to the south shore, the halocline was tilted and stratification decreased (Figure 5b). Following the salinity, bottom low DO water was advected to the south shore (Figure 5d). The up-estuary wind started to blow from about 18:00 and continued to increase to a maximum speed of 12 m/s (Figure 4a). The exchange flow was initially reversed, with upstream flow at the surface and downstream flow near the bottom (Figure 4b). Salinity stratification decreased with time until the water column became well-mixed (Figure 4d). After the salinity became uniform over the water depth, the velocity was up-estuary over

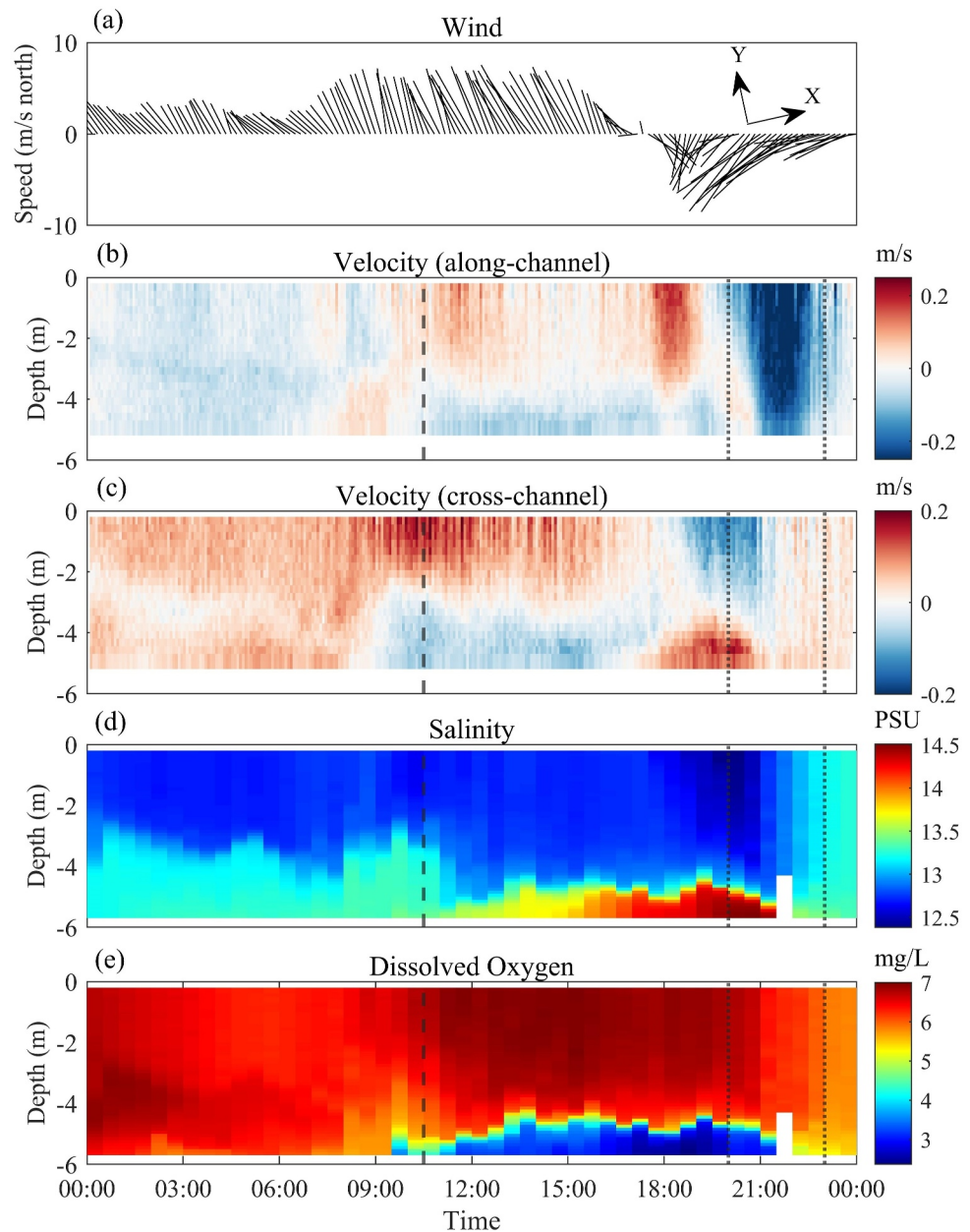


**Figure 4.** Same as Figure 3, but for 19 September. The vertical black dashed line at 10:30 is the time selected for the budget calculations for the cross-channel wind case. The black dotted lines are the times (20:00, 23:00) for the budget calculations for the up-estuary wind cases.

the entire water column. As stratification decreased, the DO in the bottom layer increased from about 3 to 5.5 mg/L when the water column became well-mixed (Figure 4e).

### 3.2. Salinity and DO Budgets From Observations

To better understand the patterns described in Section 3.1, terms of the salinity and DO budget equations were calculated at the AVP station for the first halves of each of the 2 days (black dashed lines in Figures 3 and 4) and second halves of the 2 days (black dotted lines in Figures 3 and 4). For the first halves of the 2 days, the wind had a significant cross-channel component and therefore these periods were selected to study the cross-channel wind dynamics. For the latter half of the 2 days the wind had a strong along-channel component (down-estuary for 20 June and up-estuary for 19 September) and these periods were therefore chosen to study the along-channel wind

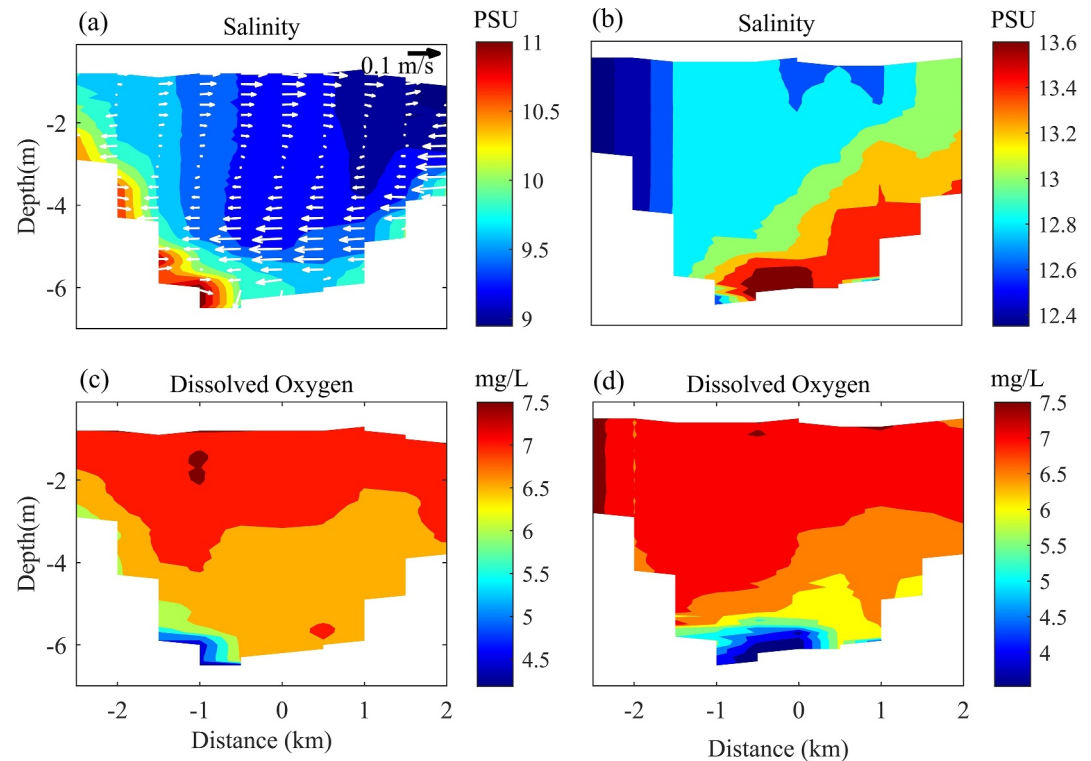


**Figure 5.** Contours of salinity and dissolved oxygen across the estuary at the central shipboard transect at 12:00 on (a, c) 20 June and (b, d) 19 September. The  $x$ -axes are lateral distances from the central Autonomous Vertical Profiler station. The left side is the north shore and the right side is the south shore; sections are views looking down-estuary. White arrows in panel (a) are the cross-channel velocities.

dynamics. The first half of the 2 days is referred to as period A, the latter half of 20 June is named period B and the latter half of the 19 September is named period C.

Vertical profiles of along-channel and cross-channel gradients of salinity and DO ( $\frac{\partial S}{\partial x}$ ,  $\frac{\partial DO}{\partial x}$ ,  $\frac{\partial S}{\partial y}$ , and  $\frac{\partial DO}{\partial y}$ ) were calculated from salinity and DO vertical profiles measured at the AVP station and adjacent shipboard stations. Because shipboard measurements were only made during the daytime, advection terms could only be calculated for period A. Vertical mixing terms were not calculated because the vertical eddy diffusivity ( $K_z$ ) was not known. In Section 3.3, the contributions of all terms of the budget equations to the evolution of the salinity and DO fields are assessed using an idealized one-dimensional model. Therefore, the time rates of change of salinity and DO ( $\frac{\partial S}{\partial t}$ ,  $\frac{\partial DO}{\partial t}$ ), longitudinal and lateral advection of salinity and DO ( $-u \frac{\partial S}{\partial x}$ ,  $-v \frac{\partial S}{\partial y}$ ,  $-u \frac{\partial DO}{\partial x}$ ,  $-v \frac{\partial DO}{\partial y}$ ) and production and respiration of DO ( $P$ ) were calculated for period A and only the time rates of change of salinity and DO ( $\frac{\partial S}{\partial t}$ ,  $\frac{\partial DO}{\partial t}$ ) and production and respiration of DO ( $P$ ) were calculated for periods B and C.

### 3.2.1. Period A Events

Cross-channel wind on both 20 June and 19 September drove strong lateral circulation and the halocline was tilted, increasing the lateral gradient of salinity. Lateral advection of salinity dominated over longitudinal advection and controlled the total rate of change of salinity (Figures 6a and 6c). Lateral advection was positive (acting to increase salinity) in the surface layer and negative (acting to decrease salinity) in the bottom layer, decreasing the vertical gradient of salinity. The positive peak in the lateral advection term at about 5-m depth (Figure 6a) was due to oscillations of the halocline, creating an opposite gradient of salinity at that depth and time. A negative cross-channel gradient of salinity at about 5-m depth can be seen in the shipboard transects around station 6, where the AVP was located (Figure 5). Although the basic patterns in the lateral advection ( $-v \frac{\partial S}{\partial y}$ ) and rate of change of salinity ( $\frac{\partial S}{\partial t}$ ) terms were similar (Figures 6a and 6c), they were not identical, suggesting that lateral advection only caused part of the observed salinity change. The residual term was

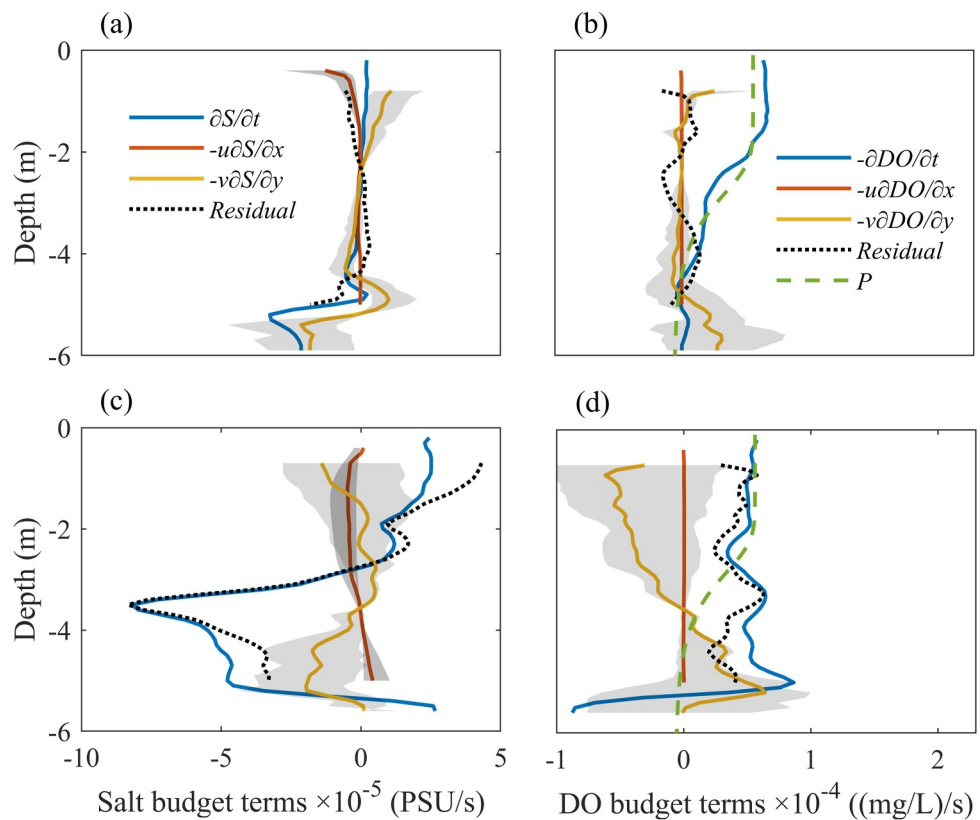


**Figure 6.** Vertical profiles of salinity and dissolved oxygen (DO) budget terms for the cross-channel wind at 10:30 on (a, b) 20 June and (c, d) 19 September. Red and yellow curves are the along- and cross-channel advection terms and the blue curve is the time rate of change of the salinity or DO concentration. The dashed green curve is the net production term, the sum of production and respiration. The dotted black curves are the residuals. The shaded areas are the uncertainties in the along- and across-channel advection.

negative in the bottom layer and positive at the surface, indicating a decrease in lower layer salinity and increase in upper layer salinity that was not accounted for in the computed advection terms. Vertical mixing, which causes vertical transport of salt from the high salinity lower layer to lower salinity upper layer may have partially contributed to the residual. However, because the depth-average of the residual is nonzero, errors in the advection terms must also contribute to the residual. The role of vertical mixing is investigated further with idealized model simulations in Section 4.3.

For the DO budget (Figures 6b and 6d), lateral advection ( $-v \frac{\partial DO}{\partial y}$ ) and production and respiration ( $P$ ) together controlled the total time rate of change of DO ( $\frac{\partial DO}{\partial t}$ ). The lateral advection terms were negative (reduced DO) in the surface layer and positive (increased DO) in the bottom layer, and thus tended to decrease the vertical oxygen gradient. Near the surface, net production ( $P$ ) was positive and much larger than the advection terms, indicating that photosynthesis dominated changes in DO in the upper water column. The production term is proportional to chlorophyll concentration which we estimated based on the average chlorophyll concentration for the lower Neuse Estuary. The chlorophyll concentration in this region typically varies by about a factor of two. However, changing chlorophyll by a factor of two does not change the budget substantively. The  $P$  term decreases with depth and becomes negative in the lower water column, due to the representation of light attenuation with depth and respiration in the expression used to calculate  $P$  (Equations 3 and 4). That is, in the bottom layer, respiration dominated over photosynthesis and the term was a sink of DO. However, the bottom DO increases with time (positive  $\frac{\partial DO}{\partial t}$ ), due to the larger positive lateral advection term. This reveals that during cross-channel wind events, lateral circulation transports higher DO water to the bottom layer and this can dominate over respiration.

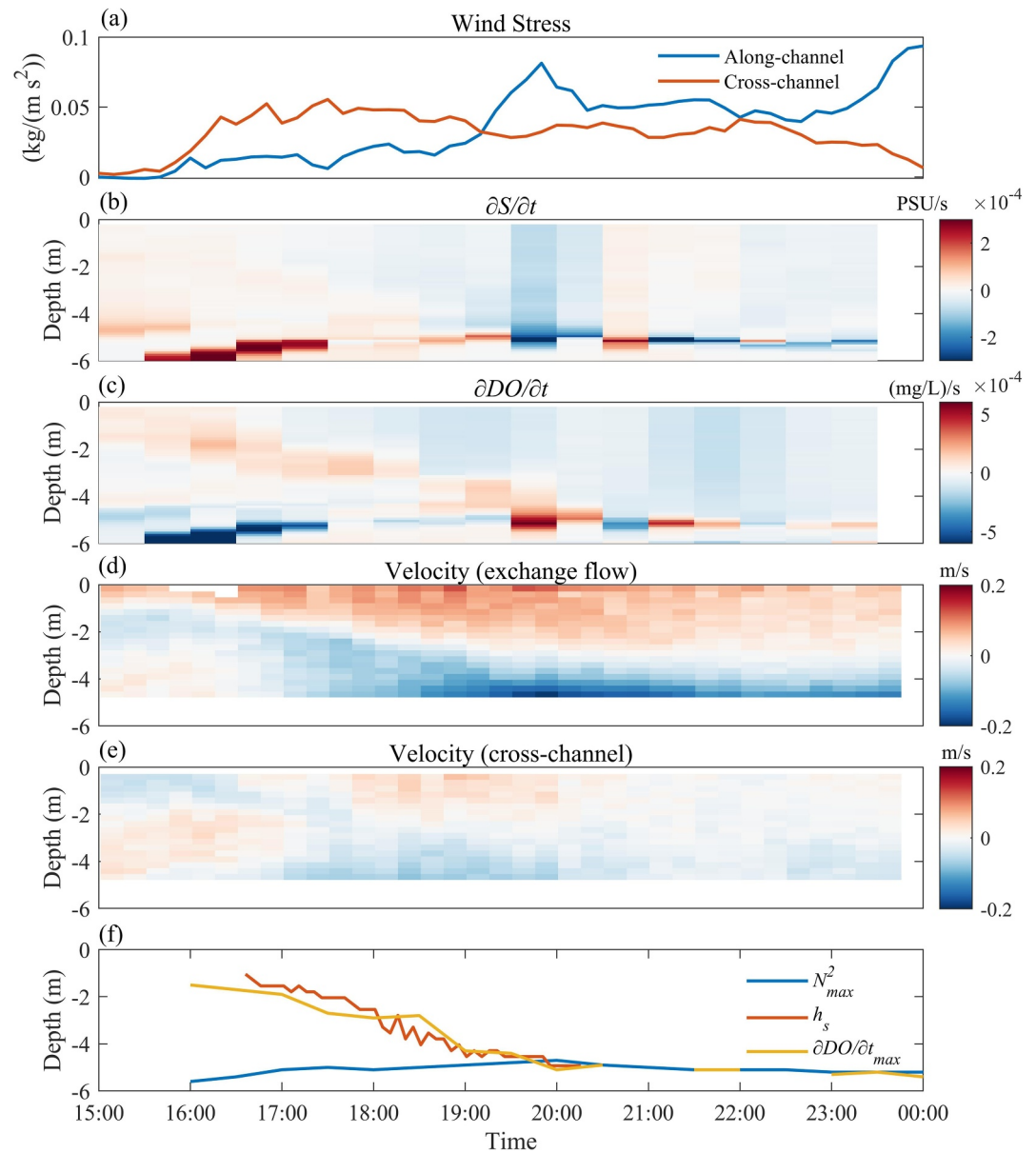


**Figure 7.** Time series of (a) wind stress, (b) time rate of change of salinity, (c) time rate of change of dissolved oxygen, (d) exchange velocity (total minus depth-average velocity), (e) cross-channel velocity and (f), depth of the highest buoyancy frequency ( $N^2$ , blue), depth of the surface outflow layer ( $h_s$ , red) and depth of the highest positive  $\frac{\partial DO}{\partial t}$  (yellow) on 20 June during the period B event.

### 3.2.2. Period B Event

During period B, the down-estuary wind stress component increased with time (Figure 7a), and three different stages can be seen in both  $\frac{\partial S}{\partial t}$  and  $\frac{\partial DO}{\partial t}$  profiles (Figures 7b and 7c). During the first stage (15:00–17:30, Figures 8a and 8b),  $\frac{\partial S}{\partial t}$  was close to zero at the surface and increased rapidly from about 5 m depth to the bottom and  $\frac{\partial DO}{\partial t}$  was positive at the surface and decreased rapidly from 5 m depth to the bottom. In this stage, the wind speed increased only slightly and lateral circulation switched directions (Figure 3c), causing relaxation of bottom high salinity and low DO water from the north shore to the measurement location in the center of the channel. This change in lateral circulation is thought to be responsible for the peak in  $\frac{\partial S}{\partial t}$  (positive) and  $\frac{\partial DO}{\partial t}$  (negative) at the bottom. This bottom peak in  $\frac{\partial S}{\partial t}$  and  $\frac{\partial DO}{\partial t}$  went away after 17:30, indicating the end of this lateral relaxation process.

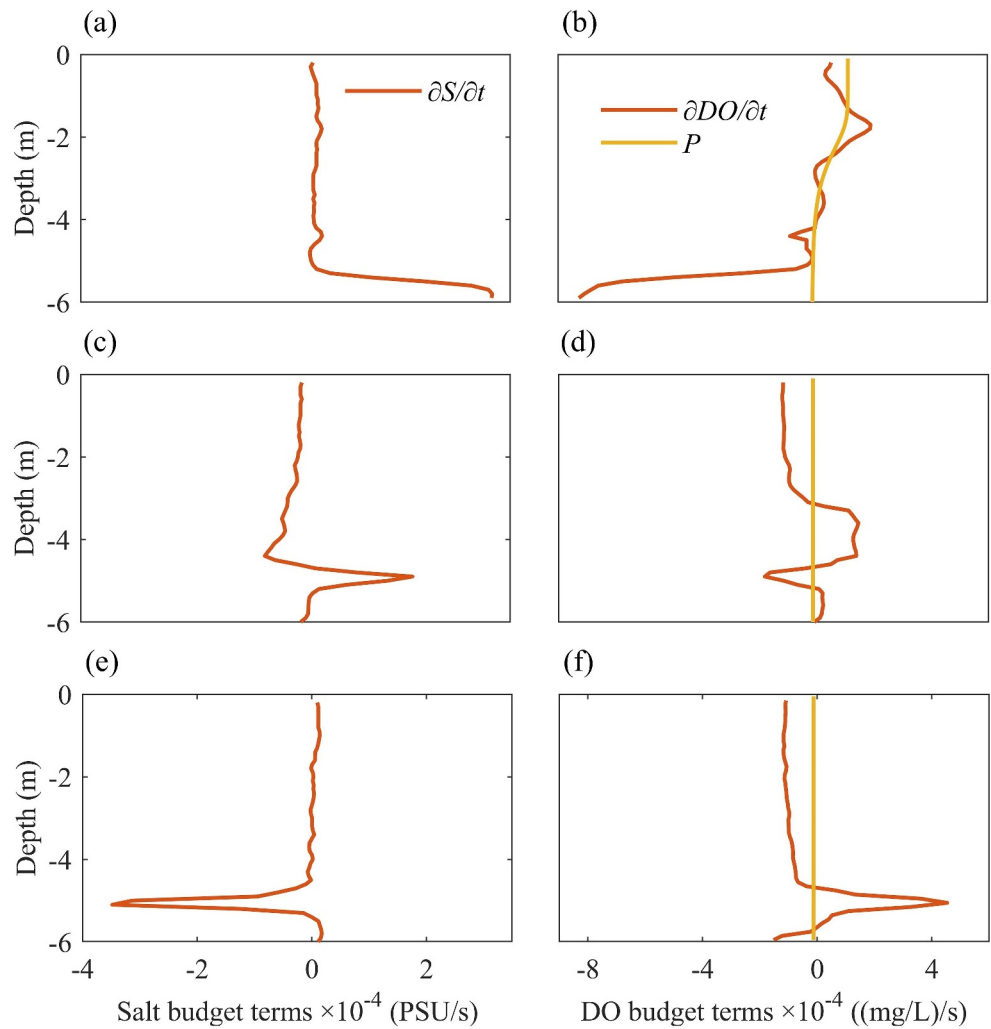


**Figure 8.** Vertical profiles of the time rate of change of (a, c, e) salinity, and (b, d, f) dissolved oxygen (red) along with production and respiration (yellow) during the down-estuary wind event at (a, b) 16:00, (c, d) 19:00 and (e, f) 21:00 on 20 June 20.

In the second stage (17:30–19:30, Figures 8c and 8d), the wind speed increased rapidly and became oriented more toward downstream, and the exchange flow increased (Figure 7d).  $\frac{\partial S}{\partial t}$  was negative in the surface layer and positive in the bottom layer; the boundary between the two layers was at about 5 m depth. This pattern is thought to be due to along-channel advection associated with the increased exchange flow. The two layers are also evident from the  $\frac{\partial DO}{\partial t}$  profiles (Figures 8b and 8d).  $\frac{\partial DO}{\partial t}$  was negative at the top and positive at the bottom of each layer, indicating vertical mixing within each layer but little exchange between the layers.

In the final stage (19:30–midnight, Figures 8e and 8f),  $\frac{\partial S}{\partial t}$  was positive at the surface and negative at the bottom and  $\frac{\partial DO}{\partial t}$  was negative at the surface and positive at the bottom. This indicates that vertical mixing dominated the salinity and DO budgets, and bottom higher salinity and lower DO water was mixed into the upper water column, tending to decrease the stratification.

In these three stages, the salinity and DO distributions were affected first by the altered lateral circulation, then by the increased exchange flow that acted to strain the along-channel salinity gradient and finally by vertical mixing. This transition is evident from the change of the surface mixed layer, the layer near the surface where momentum and dissolved materials are vertically uniform due to wind mixing (Figure 7f). The exchange flow increased over time with the increase of the wind speed, and the surface outflow layer ( $h_s$ ), defined as the layer in which the exchange flow velocity was downstream, deepened (Figures 7d and 7f). The depth of the most positive time rate

of change in DO ( $\frac{\partial DO}{\partial t}$  max) near the surface increased with time and matched  $h_s$ . Therefore,  $\frac{\partial DO}{\partial t}$  max was used to indicate the depth of the surface mixed layer.

The buoyancy frequency ( $N$ , where  $N^2 = -\frac{g}{\rho} \frac{d\rho}{dz}$ ) was calculated as an indicator of stratification. The depth of the highest  $N^2$  ( $N^2_{\max}$ ) was used to represent the depth of the strongest stratification, which separated the upper and lower salinity layers. The depth of  $N^2_{\max}$  decreased at first from 16:00 to 20:00, indicating the bottom layer thickened due to the lateral circulation and increase of the exchange flow. The surface layer thickness  $h_s$  and  $\frac{\partial DO}{\partial t}$  max deepened and met the depth of maximum stratification at 20:00, producing vertical mixing at this interface. From here the vertical mixing created by the wind eroded the stratification at the interface. The depth of  $N^2_{\max}$  then increased from 20:00 onwards and the stratification weakened.

### 3.2.3. Period C Event

During period C on 19 September, when the along-channel wind component was directed upstream, reverse exchange flow was established initially, which increased the salinity at the surface and decreased it at the bottom. The reverse exchange flow disappeared after the water column became vertically uniform (Figures 4b and 9d). The reverse exchange flow decreased the stratification, which made the water column more susceptible to vertical mixing. As the wind stress increased,  $\frac{\partial S}{\partial t}$  became more positive at the surface (salinity increasing) and more negative at the bottom (salinity decreasing) at first and then reduced to zero (Figure 9b). Advection associated with the reverse exchange flow and high vertical mixing together reduced the vertical salinity gradient until the salinity became vertically uniform. Similarly, at first  $\frac{\partial DO}{\partial t}$  became more negative at the surface and more positive at the bottom, then it reduced to zero (Figure 9c). This indicates that vertical mixing transported surface high DO water to the bottom, ultimately resulting in a uniform DO profile.

### 3.3. Salinity and DO Budgets From Idealized Simulations

It was not possible to calculate every term in the salinity and DO budgets from the field observations, so idealized simulations using GOTM were used to further evaluate the role of each term during different types of wind events. Simulations were performed with cross-estuary and up-estuary wind of 5 m/s and downstream winds of 5, 7, and 9 m/s. The simulations were run for 60 hr starting from midnight for each wind condition but run for 1 month for the 7 m/s down-estuary wind condition because the buoyancy fluxes due to wind mixing were close in size thus it took much longer time to reach steady state. Complete salinity and DO budgets were calculated based on the model output early in the simulation (after 12 hr for salinity and 7 hr for DO) and after 60 hr and 1 month to examine the steady state. The model was initialized with zero velocity thus the simulation needed some time to spin up. For this reason the salinity budget is shown after 12 hr but DO budget is shown for an earlier time (7 hr) to capture the process of increasing DO in the surface layer by photosynthesis which was dominant in the field observations.

Velocity, salinity and DO profiles during the simulations for each of the wind events are shown in Figure 10. The cross-channel wind drove lateral circulation, the halocline deepened, and the stratification decreased and finally disappeared and the water became well-mixed (Figure 10b). Following the evolution of the stratification, the bottom low DO layer also became thinner and disappeared after about 35 hr (Figure 10c). These patterns are similar to field observations from the first half of the day during 20 June and 19 September when the wind was primarily cross-channel (Figures 3d, 3e, 4d, and 4e).

For the weak (5 m/s) and moderate (7 m/s) down-estuary wind cases, the water column became more stratified with time and the halocline strengthened and deepened initially and finally ceased deepening (Figures 10e and h). Consistent with the salinity, the vertical DO gradient became stronger with time after the onset of downstream wind and the bottom layer DO decreased (Figure 10f). When the down-estuary wind was strong (9 m/s), the bottom high salinity layer thinned more rapidly and went away at about 40 hr, when the salinity profile became well-mixed (Figure 10k). The bottom low DO layer also became thinner with time (Figure 10l). These down-estuary wind cases represent the processes during the second half of the day on 20 June when the downstream component of the wind increased with time, and the stratification increased at first but decreased and finally disappeared.

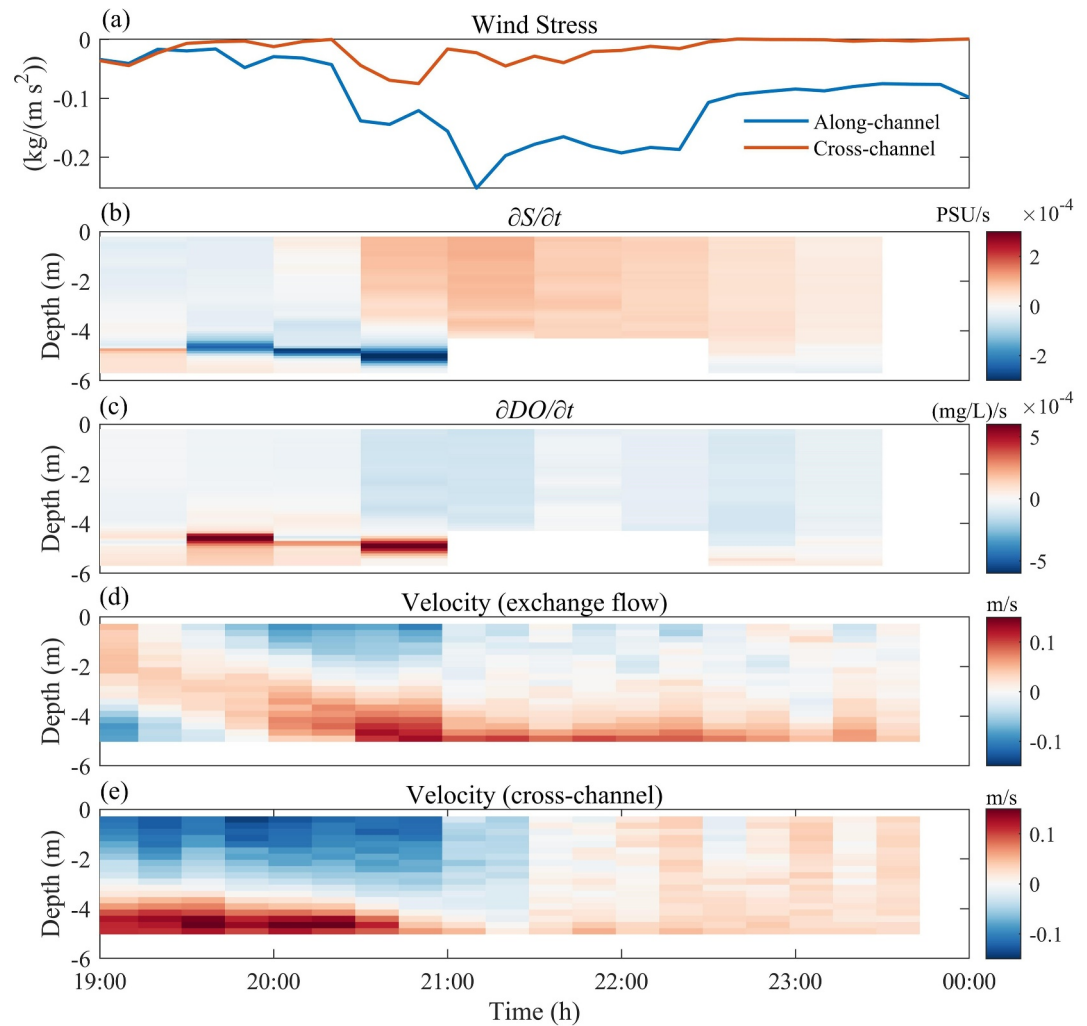


**Figure 9.** Time series of (a) along-channel and cross-channel wind stress, (b) time rate of change of salinity, (c) time rate of change of dissolved oxygen, (d) exchange velocity (actual velocity minus depth-averaged velocity) and (e) cross-channel velocity during the period C event on 19 September from 19:00 to the end of the day.

For the up-estuary wind simulation, the exchange flow was reversed, the stratification was destroyed, and the bottom low DO layer went away after about 40 hr (Figures 10m–10o). This is consistent with the observations toward the end of 19 September when the wind switched to up-estuary and the stratification and bottom low DO layer were destroyed, and the water became well-mixed.

Vertical profiles of the eddy diffusivity ( $K_z$ ) at 12 and 60 hr for four of the five wind conditions are shown in Figure 11. For the cross-channel wind, initially  $K_z$  was relatively large in the surface layer but decreased rapidly below 4 m above bottom, where the salinity started to increase. After 60 hr, the water column was well mixed (one layer) so  $K_z$  was small at the surface and bottom and large in the middle of the water column (Figure 11a). For the up-estuary wind, after 12 hr  $K_z$  was small within the layer of high stratification between 4 and 6 m above bottom. After 60 hr the salinity was uniform throughout and  $K_z$  was low at the surface and bottom and high in the middle of the water column (Figure 11b). For the 5 m/s down-estuary wind, stratification increased throughout the 60-hr simulation. There were two well-defined layers and the salinity was uniform within each layer.  $K_z$  was high in the middle of each layer and low at the top and bottom of each layer (Figure 11c). For the 9 m/s down-estuary wind, the stratification layer deepened more rapidly compared to the 5 m/s wind situation thus the low  $K_z$  layer was deeper than the 5 m/s situation. After 60 hr the water column was well-mixed and  $K_z$  was maximum in the middle of the water column, like the cross-channel and up-estuary wind situations (Figure 11d).

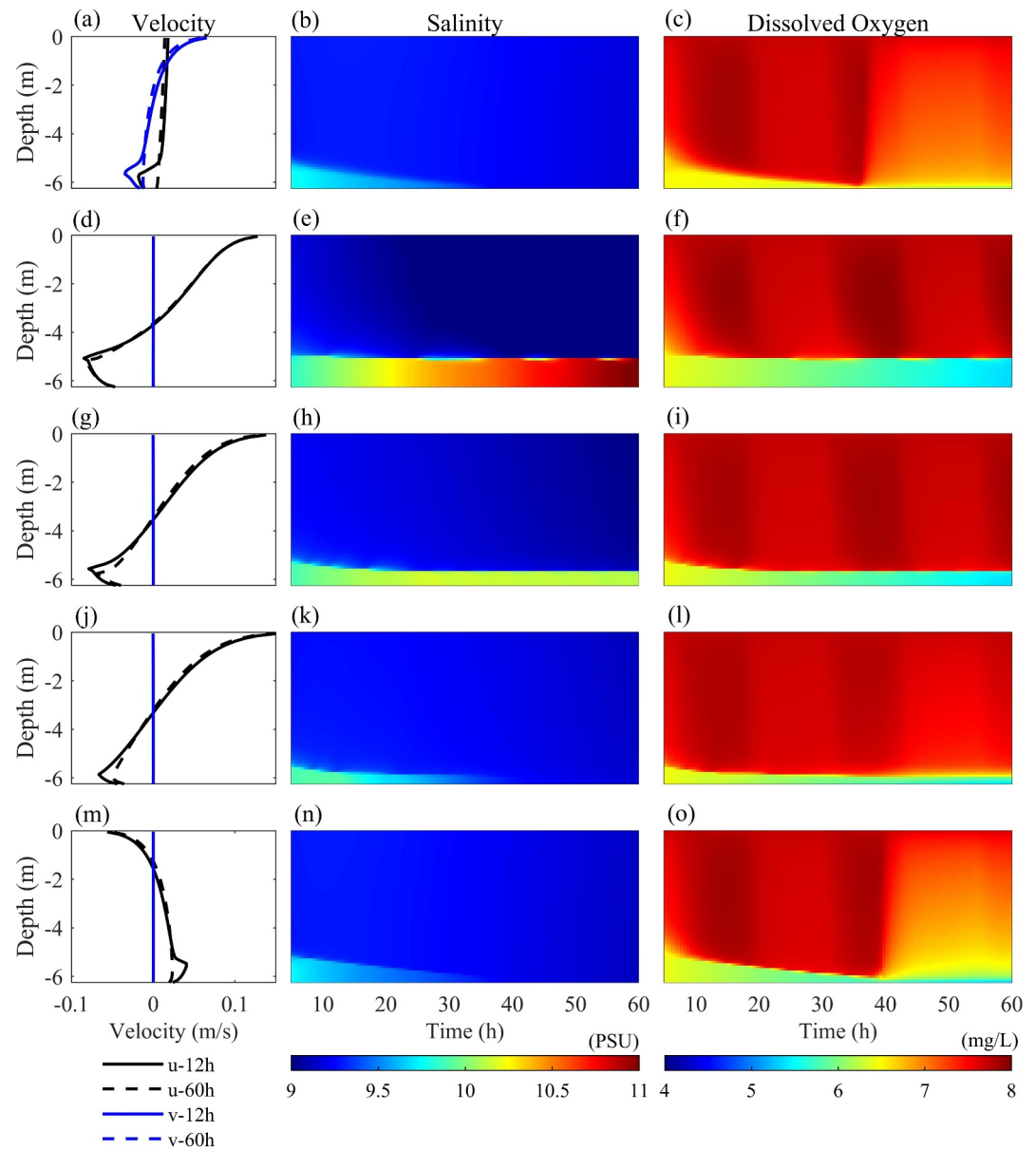


**Figure 10.** Vertical profiles of along-channel velocity and cross-channel velocity after 12 hr and 60 hr and time series of salinity and dissolved oxygen profiles from General Ocean Turbulence Model simulations with (a–c) cross-channel wind, (d–f) 5 m/s, (g–i) 7 m/s and (j–l) 9 m/s down-estuary wind and (m–o) up-estuary wind.

### 3.3.1. Cross-Estuary Wind

For the cross-channel wind simulations, lateral advection of salt dominated over longitudinal advection due to the lateral circulation forced by the wind together with the imposed lateral salinity gradient. For the 5 m/s wind, consistent with the observations, high salinity water was initially advected across the estuary in the wind direction in the upper water column and low salinity water was advected in the opposite direction in the lower water column, increasing salinity at the surface and decreasing salinity at the bottom (Figure 12a). The vertical mixing term was largest in the lower water column and it was comparable in size with the lateral advection. Lateral advection and vertical mixing together decreased the salinity at the bottom and increased it at the surface. After 60 hr (Figure 12c), the salinity profile was well mixed and  $\frac{\partial S}{\partial t}$  was constant throughout the water column and negative due to the downstream depth-averaged current, which caused loss of salt. Lateral advection was balanced by vertical mixing.

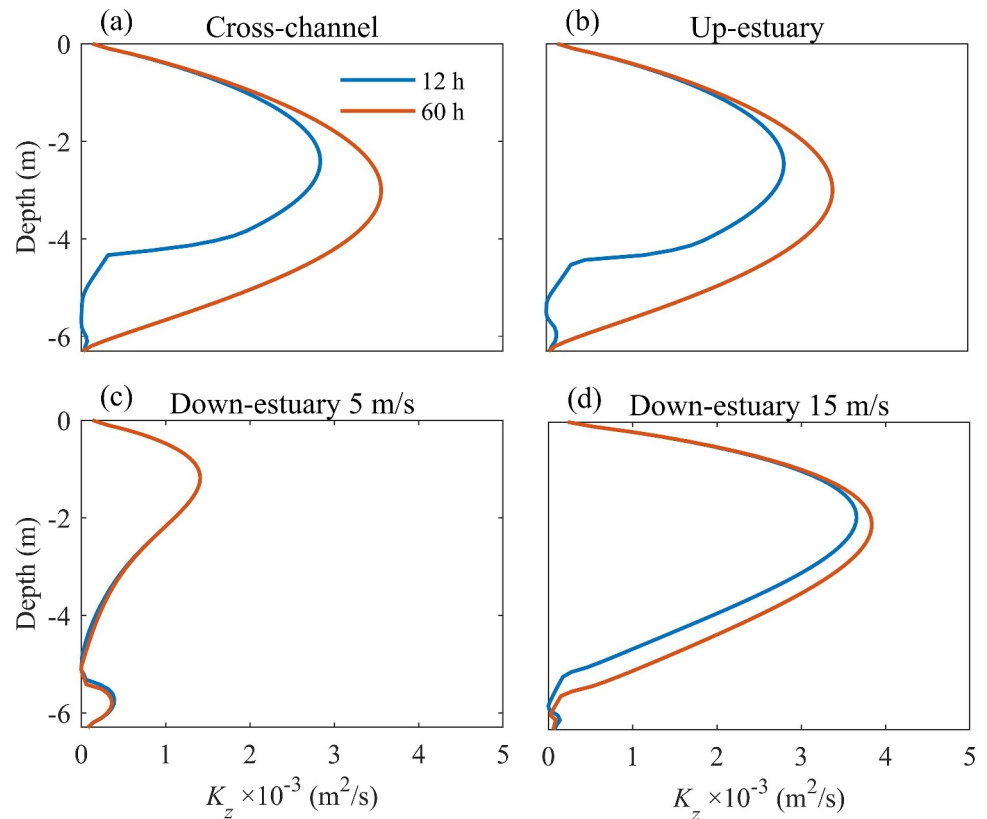


**Figure 11.** Vertical profiles of eddy diffusivity ( $K_z$ ) from General Ocean Turbulence Model simulations after 12 hr (blue) and 60 hr (red) in (a) cross-channel wind case, (b) up-estuary wind case, (c) 5 m/s down-estuary wind case and (d) 15 m/s down-estuary wind case.

For the DO budget,  $\frac{\partial \text{DO}}{\partial t}$  was positive in the surface layer due to production and vertical mixing. Vertical mixing of DO was positive in the lower layer, indicating that DO produced by photosynthesis in the upper layer was transported to the bottom layer by mixing (Figure 12b). Lateral advection also acted to increase DO in the bottom layer and decrease DO in the surface layer. After 60 hr, the water column was well-mixed and vertical mixing balanced photosynthesis and respiration (Figure 12d).

### 3.3.2. Down-Estuary Wind

Three different down-estuary wind speeds (5, 7, 9 m/s) were simulated and the salinity and DO budgets were calculated for each scenario. For the 5 m/s down-estuary wind, the salinity increased at the bottom and decreased at the surface due to along-channel advection (Figures 13a and 13c). Vertical mixing was strong in the stratified layer initially when the halocline was forming, and it balanced along-channel advection in the surface layer but was weak in the strongly stratified layer and in the bottom layer where the salinity gradient was small (Figure 13a). After the halocline ceased deepening, the vertical mixing was strong only in the surface layer where it balanced the along-channel advection and vertical mixing was weak at the halocline and bottom layer (Figure 13c). The cross-channel salinity gradient was set to zero during along-channel wind events thus the lateral advection was zero.

Consistent with the salinity, the vertical DO gradient became stronger with time. The DO increased in the surface layer due to the  $P$  term and vertical mixing. Vertical mixing was strong in the surface layer and top of the bottom low DO layer when it was still forming and was weak in the layer of strong stratification that separated the upper and lower layers. DO decreased in the bottom layer due to respiration and vertical mixing combined with SOD (Figure 13b). After 60 hr when the bottom layer was well-formed and anoxic, vertical mixing was weak in the stratified layer and bottom layer (Figure 13d). In the surface layer, vertical mixing brought the DO produced by photosynthesis to the lower part of the surface layer which was below the euphotic zone.

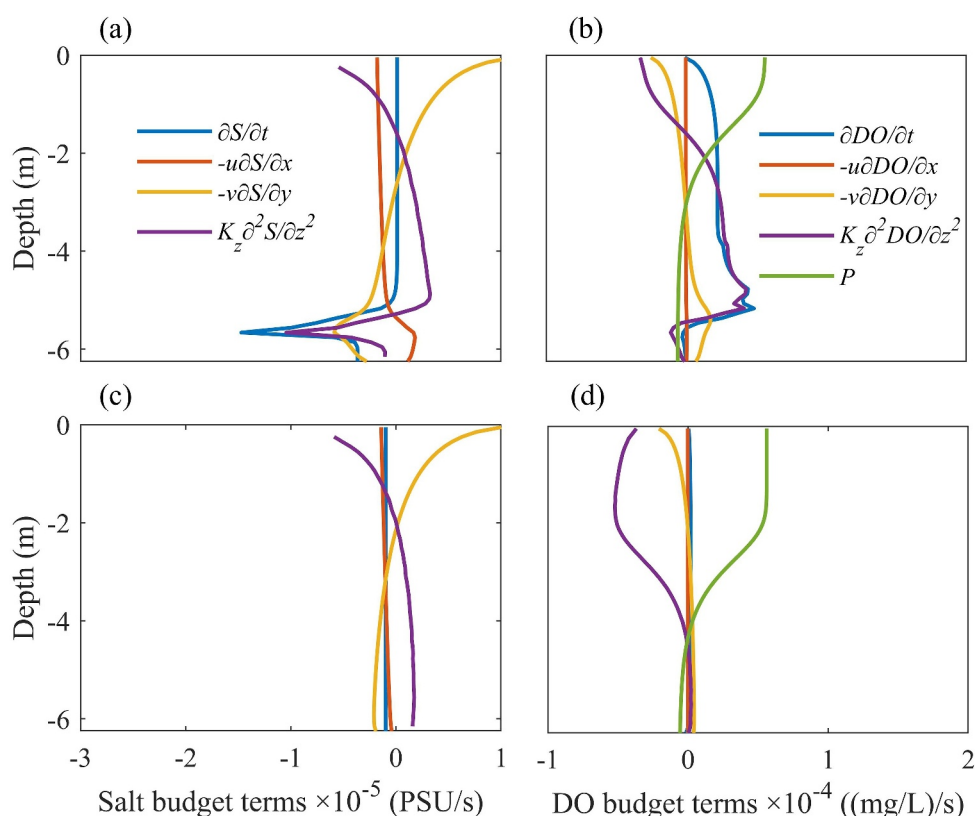


**Figure 12.** Vertical profiles of salinity budget terms from General Ocean Turbulence Model simulations of cross-estuary wind after (a) 12 hr and (c) 60 hr and dissolved oxygen budget at (b) 7 hr and (d) 60 hr.

For the 7 m/s down-estuary wind, the bottom layer became thinner with time after the start of the simulation. The salinity decreased at the surface and increased at the bottom due to along-channel advection, creating a strong halocline. Vertical mixing was strong initially in the stratified layer when the halocline was still deepening. In the end, vertical mixing was strong in the surface layer where it balanced along-channel advection and it was much smaller in the stratified layer and bottom layer (Figure 14a). For the DO budget, vertical mixing was strong in the surface layer and top of the bottom low DO layer when it was still forming and mixing was weak in the stratified layer. In the end, the vertical mixing was strong enough in the surface layer to bring the DO produced by photosynthesis to the lower part of the surface layer. Mixing was weak in the stratified layer and within the bottom layer (Figure 14b).

When the wind was 9 m/s toward down-estuary, the water column became well mixed by the end of the simulation. After the water column was well-mixed, vertical mixing diffused bottom high salinity water to the upper water column and along-channel advection transported salt out of this location, causing a net loss of the salt (Figure 14c). For the DO budget, vertical mixing transported DO from the surface toward the bottom. The DO reached a steady state in which  $P$  was balanced by vertical mixing (Figure 14d).

In conclusion, down-estuary wind initially acted to increase the exchange flow, strain the salinity field, and enhance stratification and decrease bottom DO. For small wind speeds, a steady state was reached in which the surface mixed layer stopped deepening. For larger wind speeds, the surface layer deepened and the bottom layer became thinner. After some time, the effects of wind mixing exceeded the wind straining and the whole water column became well mixed.

### 3.3.3. Up-Estuary Wind

For the up-estuary wind simulations, the wind always acted primarily to mix the water column, decreasing the stratification and generating vertical mixing. Salinity initially decreased at the bottom and increased at the

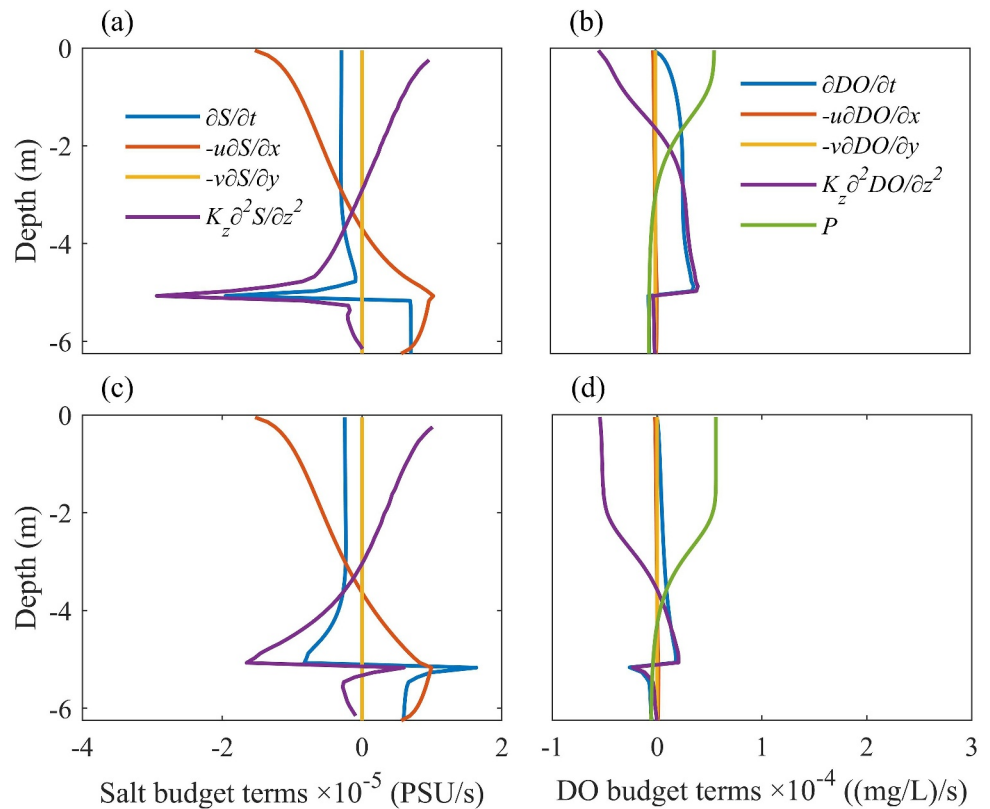


**Figure 13.** Vertical profiles of salinity budget terms from General Ocean Turbulence Model simulations of 5 m/s down-estuary wind after (a) 12 hr and (c) 60 hr and dissolved oxygen budget at (b) 7 hr and (d) 60 hr.

surface due to along-channel advection and vertical mixing. Vertical mixing occurred within each layer and was strongest in the stratified layer separating the upper and lower layers, acting to erode the stratification (Figure 15a). After 60 hr (Figure 15c), the salinity profile became uniform and along-channel advection due to the reversed exchange flow was balanced by convective vertical mixing throughout the water column. DO increased in the stratified layer separating the upper and lower layers due to the high vertical mixing (Figure 15b). Along-channel advection was weak compared to vertical mixing because of the weak along-channel gradient of DO. After 60 hr when the salinity was well-mixed, the DO reached a steady state in which vertical mixing balanced  $P$  (Figure 15d).

## 4. Discussion

### 4.1. Influence of Wind Direction and Speed on Salinity and Oxygen Dynamics

The response of the salinity and DO fields to wind is distinct for different wind direction relative to the channel. For along-channel wind, the relative sign of the salinity gradient and wind stress determines whether the wind straining increases stratification and hence opposes vertical mixing (down-estuary wind) or wind straining decreases stratification and hence promotes vertical mixing (up-estuary wind). For the along-channel wind cases, the length scale of the channel is large so there is not significant isohaline tilt in response to the wind. In contrast, the scale of channel width is small in the cross-channel direction and therefore cross-channel wind results in a halocline tilt which affects the baroclinic pressure gradient and hence the lateral velocities and advection.

Lateral circulation can be driven by wind and modulates the salinity and DO profile simultaneously. In this study, we observed lateral circulation driven by cross-estuary winds that acted to tilt isopycnals, and thus reduce vertical stratification and increase bottom DO. This differs from previous work in the Chesapeake Bay that reported lateral circulation driven by along-channel winds. Li and Li (2012) showed, from model simulations in the Chesapeake Bay, along-channel winds drive lateral circulation due to the cross-channel Ekman transport. Isopycnals are tilted

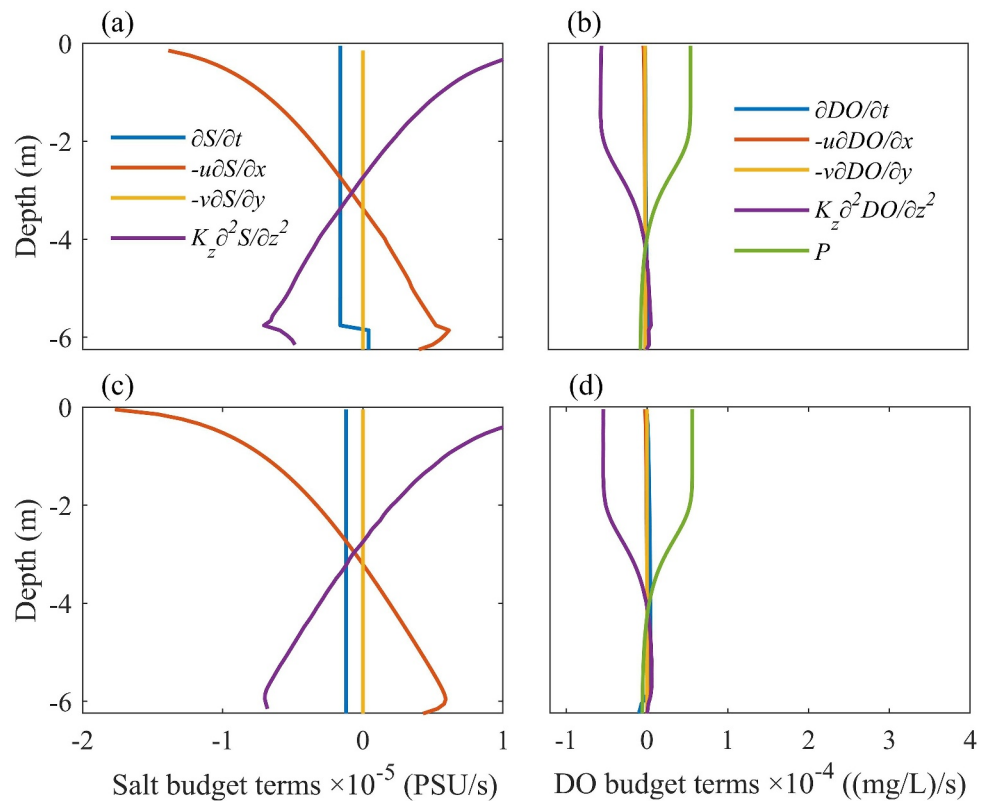


**Figure 14.** Vertical profiles of salinity budget (Equation 1) and dissolved oxygen budget (Equation 2) terms from idealized simulations at 1 month for (a, b) 7 m/s and 60 hr for (c, d) 9 m/s down-estuary wind scenarios.

in the across-channel direction, which creates a lateral baroclinic pressure gradient that interacts with the Ekman transport. In the Neuse Estuary, the average water depth (<4 m) is much less than the typical Ekman layer thickness (Csanady, 1967). The central station in the study area (AVP station) is located in the straight part of the lower Neuse estuary and far away from the bend, thus the dynamics at this location are not directly affected by the channel curvature. Thus, the lateral circulation observed in this study is primarily driven by the cross-channel winds. Reynolds-Fleming and Luettich (2004) measured salinity and DO profiles at each side of the upper leg of the Neuse Estuary and found a correspondence between high salinity and low DO in the bottom water on each side of the estuary under cross-channel winds. The present study provides a more complete view of salinity and DO cross-sections and cross-estuary circulation under different wind conditions. The bottom high salinity and low DO layer is clearly shown to be advected to the side of the estuary due to lateral circulation under cross-channel winds. Furthermore, salinity and DO budgets show that lateral circulation causes lateral advection that decreases the vertical salinity gradient. This promotes vertical mixing, which combines with lateral advection to make the salinity and DO profiles vertically uniform.

Along-channel winds not only serve as an energy source for turbulent mixing but can also alter the exchange flow and strain the along-channel salinity gradient to modify vertical stratification. Scully et al. (2005) found that in the York River Estuary in Virginia, down-estuary winds enhance the exchange flow, strain the along-channel density field and increase the stratification while up-estuary winds reduce them. In our study, reversed exchange flow was observed during up-estuary winds, causing advection that decreased the stratification ultimately leading to high vertical mixing. Chen and Sanford (2009) simulated an idealized estuary and found that the exchange flow and stratification first increase then decrease as down-estuary wind speed increases. In this study, both the observations and model results capture the deepening of the surface mixed layer after the onset of down-estuary wind. From observations, as the wind increased, the exchange flow and stratification increased at first and then decreased and finally disappeared after the surface mixed layer reached the stratification layer and created strong vertical mixing.

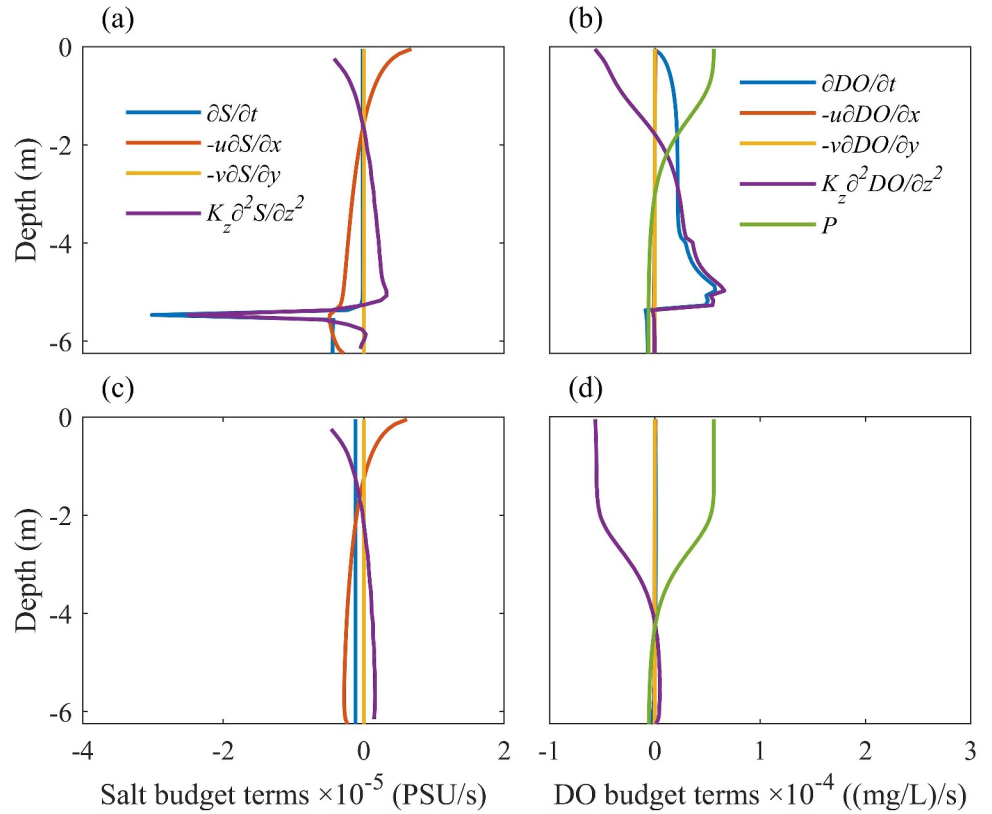


**Figure 15.** Vertical profiles of salinity (Equation 1) and dissolved oxygen (Equation 2) budget terms derived from 1D idealized model simulations with up-estuary wind. (a, b) After 12 hr and (c, d) after 60 hr.

The simulations further reveal that the bottom high salinity layer is thinner for larger wind speeds, as wind mixing penetrates deeper into the water column. Under small and moderate speeds (5 and 7 m/s), the deepening of the surface layer eventually stops and beyond this time wind acts primarily to strain the along-estuary salinity gradient and increases the density difference between upper and lower layers in the two-layer stratification. Only when the wind stress exceeds a threshold (9 m/s case) does vertical mixing dominate over straining all the way to the bottom. Chen and Sanford (2009) derived a modified horizontal Richardson number ( $Ri_{x,new}$ ), a ratio of generation of buoyancy by straining of the along-estuary salinity gradient ( $B_{shear}$ ) to vertical buoyancy flux due to turbulent mixing ( $B_{turb}$ ) to include the effects of wind on the estuarine circulation and vertical mixing. The expression is:

$$(Ri_{x,new})^2 = \frac{B_{shear}}{B_{turb}} \sim \frac{(H^4 N_x^4 / 48 K_M)(1 - W)}{R_f (u_{*s}^3 / \kappa h_s + u_{*b}^3 / \kappa h_b)} \quad (9)$$

where the  $N_x^2$  is the longitudinal buoyancy frequency,  $K_M$  is the effective eddy viscosity,  $W = \frac{\tau_x L}{\Delta \rho g H^2}$  is the Wedderburn number,  $\tau_x$  is the along-channel wind stress,  $\Delta \rho / L$  is the along-channel density gradient,  $H$  is the water depth,  $R_f$  is the flux Richardson number (Ivey & Imberger, 1991),  $u_{*s}$  and  $u_{*b}$  are surface and bottom friction velocities,  $h_s$  and  $h_b$  are surface and bottom layer thicknesses and  $\kappa$  is the von Kármán constant (0.41). The wind straining dominates over mixing when  $Ri_{x,new} > 1$  and vice versa.

We calculated  $Ri_{x,new}$  from both the model output at steady state and our field observations following Chen and Sanford (2009), using  $R_f = 0.2$ , which is a typically used maximum value (Ivey & Imberger, 1991). The  $N_x^2$  was calculated based on  $\frac{\partial S}{\partial x}$ ,  $h_s$  and  $h_b$  were estimated from the model and observation profiles (Figures 3 and 10),  $K_M$  scales as  $a_0 C'_d UL$  where  $a_0$  is 0.028,  $C'_d$  is bottom drag coefficient ( $5.5 \times 10^{-3}$ ),  $U$  is the velocity at 1 m above



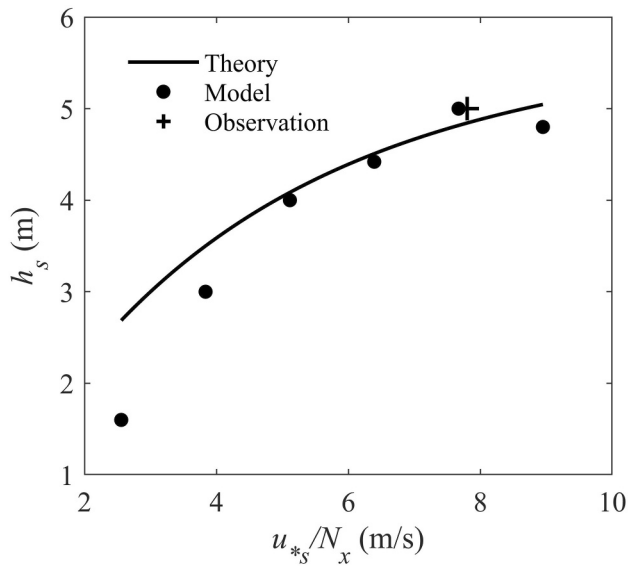


**Figure 17.** Comparison of surface boundary layer thickness ( $h_s$ ) predicted by theory (Equation 13) with observational data (20:00 to 24:00 on 20 Juneth) and 1D model simulations.

The solution for  $h_s$  is:

$$h_s = \frac{-g \frac{\partial \eta}{\partial x} + \sqrt{\left(g \frac{\partial \eta}{\partial x}\right)^2 + \frac{2g}{\rho} \frac{\partial \rho}{\partial x} \frac{\tau_s}{\rho}}}{\frac{g}{\rho} \frac{\partial \rho}{\partial x}} \quad (13)$$

The  $\frac{g}{\rho} \frac{\partial \rho}{\partial x}$  term is the horizontal buoyancy frequency ( $N_x^2$ ). Note that in the above derivation it is implicit that the surface slope is in response to the wind stress and therefore differs from the surface slope associated with the imposed inflow. To quantify  $-g \frac{\partial \eta}{\partial x}$ , we consider a simplified depth-averaged momentum budget in which there is a balance between wind stress and barotropic pressure gradient, and the baroclinic pressure gradient and bottom friction are neglected for simplicity. Therefore  $-g \frac{\partial \eta}{\partial x}$  is estimated as  $-\frac{\tau_s}{\rho H} = -\frac{u_*s^2}{H}$  where  $H$  is the water depth. Substituting this into Equation 13 yields the final expression for  $h_s$ :

$$h_s \sim \frac{u_*s^2}{N_x^2 H} \left[ -1 + \sqrt{1 + 2 \left( \frac{N_x H}{u_*s} \right)^2} \right] \quad (14)$$

To compare this prediction of  $h_s$  with the model results, a series of wind scenarios (from 2 to 7 m/s at intervals of 1 m/s) were run in GOTM (Figure 17). The model predictions match the theory well, particularly for the larger wind speeds. The theoretical value is larger than the model results under small wind speeds (2, 3 m/s) due to overestimation of  $-g \frac{\partial \eta}{\partial x}$  because the baroclinic and bottom stress terms are not negligible for these small wind speed cases. Averaged  $h_s$  from the observations between 20:00 to 24:00 20 June, when  $h_s$  was relatively stable, is in line with the simulation results and the theory.

### 4.3. Combined Influence of Biological and Physical Processes on DO Dynamics

DO dynamics are influenced by physical processes (advection, mixing) in a similar way to the salinity dynamics, but are also influenced by biological processes. Scully (2010b) simulated the changes of the total volume of bottom hypoxic water under different wind conditions in the Chesapeake Bay. Their goal was to isolate the role of physical processes in oxygen dynamics by assuming the biological processes are constant in both time and space. They used a constant respiration rate throughout the estuary, and no photosynthesis or SOD. They found that winds coming from all directions tend to decrease the bottom hypoxic volume, although the extent differs. Lateral circulation due to Ekman transport and vertical mixing caused by the decrease of stratification are two dominant reasons.

In this study, diurnally varying photosynthesis and SOD were taken into account, and the focus is the processes that control vertical profiles of DO over much shorter time-scales (hours and days). Photosynthesis in the surface layer tends to increase the vertical gradient of the DO during the daytime, which contributes to a higher vertical turbulent DO flux that can increase the bottom layer DO concentration. Sediment oxygen demand at the bottom boundary creates a vertical gradient of DO close to the seabed, thus vertical mixing transports DO downward to the seabed, decreasing bottom layer DO. When deepening of the surface mixed layer is arrested because surface layer turbulence cannot overcome stratification at the interface between upper and lower layers generated by straining of the along-channel salinity gradient (5 and 7 m/s down-estuary wind scenarios), the turbulent flux of DO through the halocline is weaker than respiration and SOD, and the bottom layer DO concentration decreases. When wind-induced mixing is able to penetrate the full water depth (9 m/s down-estuary wind and up-estuary wind scenarios), vertical mixing of DO is stronger than the combined SOD and bottom layer respiration, increasing the bottom layer DO. Lateral advection caused by lateral circulation is strong under cross-channel winds and combines with vertical mixing to increase the bottom DO.

#### 4.4. Response of Stratification and Bottom DO to Wind Over 6-Month Deployment

The responses of the salinity and DO distributions to wind events in the Neuse follow some general patterns. The bottom high salinity region generally corresponds with the bottom low DO region. Wind causes an increase in stratification and decrease in bottom DO only under small and moderate down-estuary winds. For all the other wind directions and speeds, wind tends to decrease the stratification and increase bottom DO, although the mechanisms differ depending on wind direction.

There are several interesting exceptions to these general patterns in the observations. One exception is the event between 15 to 16 June (second black box in Figure 2). The wind blew toward downstream and the bottom DO decreased at first but quickly increased again even though the stratification kept increasing. Because the patterns in salinity and DO are different, this decrease in DO is clearly the result of advection rather than vertical mixing. This might result from a change in the horizontal gradient of the DO, meaning the exchange flow brought higher DO water to the bottom of the study area through along-channel advection. Another exception is the event from 20 to 21 June discussed above (third black box in Figure 2). During this event, the downstream wind strength and duration were sufficient that the surface mixed layer continued to thicken and wind mixing ultimately eroded the stratification completely.

The cross-channel wind component was usually less important than the along-channel wind component for the stratification and DO dynamics as  $\Delta S$  and bottom DO are better correlated to along-channel components than cross-channel components in this 6-month period. But the effect of the lateral circulation to increase bottom DO can become dominant when the along-channel component is weak or the cross-channel component is strong. A typical example is the event between 11 and 12 June (first black box in Figure 2). The wind switched from upstream to downstream but at the same time the cross-channel part of the wind increased rapidly and became sufficiently strong that the homogenizing effect of the cross-channel wind component dominated over the straining effect of the downstream wind component, so stratification decreased and bottom DO increased. Another example of dynamics driven by the cross-channel wind component is the event between 24 and 28 June when the cross-channel wind component switched from positive to negative,  $\Delta S$  increased and then decreased, and the bottom DO decreased and then increased. The bottom high salinity and low DO layer was presumably forced from one side of the estuary to the other side. The isopycnals and oxyclines relaxed initially, increasing stratification and decreasing the bottom DO locally, and then tilted in the opposite direction to decrease the stratification and increase the bottom DO.

The responses of salinity and DO to wind events in the Neuse Estuary are complex, and many exceptions to the general patterns emphasized in this manuscript occurred during the 6-month deployment. Both the wind and circulation vary with time, and wind events cause responses in the circulation (e.g., seiches) that extend beyond the length of the wind event. The response of the circulation to wind depends on the stratification and horizontal salinity gradients at that time, which is established by the history of wind and inflow in the estuary. Also, when the wind is not purely along- or cross-channel, the interaction of these two parts together determines the hydrodynamics and DO dynamics in the estuary, and this is a topic that requires further study.

## 5. Conclusions

Our analyses of field measurements and idealized 1D simulations found distinct effects of the wind on salinity and DO dynamics that depended on wind direction and speed. Cross-channel wind drives lateral circulation and tilts isohalines and oxyclines, creating lateral advection and vertical mixing that together decrease stratification and increase bottom DO. Down-estuary wind can increase or decrease the exchange flow and stratification, depending on the wind speed and duration. After the onset of down-estuary wind, the exchange flow increases, driving along-channel advection that strengthens the stratification and decreases bottom DO. After the onset of wind, the surface boundary layer deepens with time and interacts with the stratification. Surface mixed layer deepening is halted at some depth due to the straining of the along-estuary density gradient by the exchange flow. An expression for the surface layer thickness at steady state ( $h_s$ ) derived by considering the competition between horizontal and vertical buoyancy flux over the surface layer matches the model output and observations well. For faster wind speeds, vertical mixing erodes the stratification completely and penetrates the full water depth, and bottom DO increases. Up-estuary wind decreases and can even reverse the exchange flow, creating opposite along-channel advection and promoting vertical mixing that homogenizes the salinity and DO profiles.

Analysis of our 6-month data set illustrates that, while the patterns described above generally hold for purely across- or along-channel wind events, wind effects on estuarine dynamics and hypoxia are considerably more complex than this idealized picture because the wind direction can be at any angle to the estuarine axis and varies continuously with time. Additionally, the biological processes of photosynthesis, respiration and SOD are known to vary in space and time, and significantly affect the DO budget and distribution. While this study illustrates that wind can profoundly affect salinity and DO distributions in estuaries both directly, through wind mixing and advection by wind-driven along-estuary and lateral circulation, and indirectly through straining of the density field which modifies stratification and hence vertical mixing, further work on complexities due to combinations of along- and cross-channel wind components, histories of wind and river flow, and biological processes is clearly needed.

### Data Availability Statement

Observational datasets and model input files are available at <https://doi.org/10.5061/dryad.7sqv9s4zh>. ModMon data can be accessed through the Southeast Coastal Ocean Observing Regional Association data portal at <https://portal.secoora.org/#metadata/190/affiliate>.

### Acknowledgments

We thank Ryan Neve and David Marshall for help with all aspects of the field measurements, Patrick Combe and Xiao Yu who assisted with shipboard ADCP/CTD measurements, and Glenn Safrit who helped with scientific diving. Funding for this research came from the NCDEQ Coastal Recreational Fishing License Grant Program, the Joseph S. Ramus Endowment Fund, and the National Science Foundation Physical Oceanography program (OCE-2421659 and OCE-2421660). We are grateful to Nicholas Nidzicko and one anonymous reviewer for thoughtful comments that improved this manuscript.

### References

- Altieri, A. H., & Gedan, K. B. (2015). Climate change and dead zones. *Global Change Biology*, 21(4), 1395–1406. <https://doi.org/10.1111/gcb.12754>
- Blanton, J. O., Amft, J. A., Lee, D. K., & Riordan, A. (1989). Wind stress and heat fluxes observed during winter and spring 1986. *Journal of Geophysical Research*, 94(C8), 10686–10698. <https://doi.org/10.1029/JC094iC08p10686>
- Breitburg, D., Levin, L. A., Oschlies, A., Grégoire, M., Chavez, F. P., Conley, D. J., et al. (2018). Declining oxygen in the global ocean and coastal waters. *Science*, 359(6371), eaam7240. <https://doi.org/10.1126/science.aam7240>
- Buzzelli, C. P., Luettich, R. A., Jr., Paerl, H. W., Fear, J., Fleming, J., Twomey, L., et al. (2002). *Neuse River Estuary modeling and monitoring project phase 2: Monitoring of hydrography and water quality, circulation, phytoplankton physiology and sediment-water coupling*. Water Resources Research Institute of the University of North Carolina.
- Buzzelli, C. P., Luettich, R. A., Jr., Powers, S. P., Peterson, C. H., McNinch, J. E., Pinckney, J. L., & Paerl, H. W. (2002). Estimating the spatial extent of bottom-water hypoxia and habitat degradation in a shallow estuary. *Marine Ecology Progress Series*, 230, 103–112. <https://doi.org/10.3354/meps230103>
- Chant, R. J., Geyer, W. R., Houghton, R., Hunter, E., & Lerczak, J. A. (2007). Estuarine boundary layer mixing processes: Insights from dye experiments. *Journal of Physical Oceanography*, 37(7), 1859–1877. <https://doi.org/10.1175/JPO3088.1>
- Chen, S.-N., & Sanford, L. P. (2009). Axial wind effects on stratification and longitudinal salt transport in an idealized, partially mixed estuary. *Journal of Physical Oceanography*, 39(8), 1905–1920. <https://doi.org/10.1175/2009jpo4016.1>
- Coogan, J., & Dzwonkowski, B. (2018). Observations of wind forcing effects on estuary length and salinity flux in a river-dominated, microtidal estuary, Mobile Bay, Alabama. *Journal of Physical Oceanography*, 48(8), 1787–1802. <https://doi.org/10.1175/JPO-D-17-0249.1>
- Csanady, G. T. (1967). On the “resistance law” of a turbulent Ekman layer. *Journal of the Atmospheric Sciences*, 24(5), 467–471. [https://doi.org/10.1175/1520-0469\(1967\)024<0467:OTLOAT>2.0.CO;2](https://doi.org/10.1175/1520-0469(1967)024<0467:OTLOAT>2.0.CO;2)
- Cui, Y., Wu, J., Ren, J., & Xu, J. (2019). Physical dynamics structures and oxygen budget of summer hypoxia in the Pearl River Estuary. *Limnology & Oceanography*, 64(1), 131–148. <https://doi.org/10.1002/lno.11025>
- Diaz, R. J. (2001). Overview of hypoxia around the world. *Journal of Environmental Quality*, 30(2), 275–281. <https://doi.org/10.2134/jeq2001.302275x>
- Diaz, R. J., & Rosenberg, R. (2008). Spreading dead zones and consequences for marine ecosystems. *Science*, 321(5891), 926–929. <https://doi.org/10.1126/science.1156401>
- Hagy, J. D., Boynton, W. R., Keefe, C. W., & Wood, K. V. (2004). Hypoxia in Chesapeake Bay, 1950–2001: Long-term change in relation to nutrient loading and river flow. *Estuaries*, 27(4), 634–658. <https://doi.org/10.2307/1353476>
- Hench, J. L., Bircher, J. T., & Luettich, R. A., Jr. (2000). A portable retractable ADCP boom-mount for small boats. *Estuaries*, 23(3), 392–399. <https://doi.org/10.2307/1353331392-399>
- Ivey, G. N., & Imberger, J. (1991). On the nature of turbulence in a stratified fluid. Part I: The energetics of mixing. *Journal of Physical Oceanography*, 21(5), 650–658. [https://doi.org/10.1175/1520-0485\(1991\)021<0650:OTNOTI>2.0.CO;2](https://doi.org/10.1175/1520-0485(1991)021<0650:OTNOTI>2.0.CO;2)
- Jassby, A. D., & Platt, T. (1976). Mathematical formulation of the relationship between photosynthesis and light for phytoplankton. *Limnology & Oceanography*, 21(4), 540–547. <https://doi.org/10.4319/lno.1976.21.4.0540>
- Kato, H., & Phillips, O. M. (1969). On the penetration of a turbulent layer into stratified fluid. *Journal of Fluid Mechanics*, 37(4), 643–655. <https://doi.org/10.1017/s0022112069000784>
- Keeling, R. F., Körtzinger, A., & Gruber, N. (2010). Ocean deoxygenation in a warming world. *Annual Review of Marine Science*, 2(1), 199–229. <https://doi.org/10.1146/annurev.marine.010908.163855>
- Ladwig, R., Rock, L. A., & Dugan, H. A. (2021). Impact of salinization on lake stratification and spring mixing. *Limnology and Oceanography Letters*, 8(1), 93–102. <https://doi.org/10.1002/lol2.10215>
- Lange, X., & Burchard, H. (2019). The relative importance of wind straining and gravitational forcing in driving exchange flows in tidally energetic estuaries. *Journal of Physical Oceanography*, 49(3), 723–736. <https://doi.org/10.1175/jpo-d-18-0014.1>
- Large, W. G., & Pond, S. (1981). Open ocean momentum flux measurements in moderate to strong winds. *Journal of Physical Oceanography*, 11(3), 324–336. [https://doi.org/10.1175/1520-0485\(1981\)011<0324:OOMFMI>2.0.CO;2](https://doi.org/10.1175/1520-0485(1981)011<0324:OOMFMI>2.0.CO;2)
- Lee, Y. J., & Lwiza, K. M. M. (2008). Characteristics of bottom dissolved oxygen in long Island Sound, New York. *Estuarine, Coastal and Shelf Science*, 76(2), 187–200. <https://doi.org/10.1016/j.ecss.2007.07.001>
- Li, Y., & Li, M. (2012). Wind-driven lateral circulation in a stratified estuary and its effects on the along-channel flow. *Journal of Geophysical Research*, 117, C09005. <https://doi.org/10.1029/2011jc007829>

- Luettich, R. A., McNinch, J. E., Paerl, H. W., Peterson, C. H., Wells, J. T., Alperin, M. J., et al. (2000). Neuse River estuary modeling and monitoring project stage 1: Hydrography and circulation, water column nutrients and productivity, sedimentary processes and benthic-pelagic coupling. In *Water Resources Research Institute of the University of North Carolina, Report UNC-WRRI-2000-325B* (p. 172).
- Mellor, G. L., & Yamada, T. (1982). Development of a turbulence closure model for geophysical fluid problems. *Reviews of Geophysics*, 20(4), 851–875. <https://doi.org/10.1029/RG020i004p00851>
- Officer, C. B., Biggs, R. B., Taft, J. L., Cronin, L. E., Tyler, M. A., & Boynton, W. R. (1984). Chesapeake Bay anoxia: Origin, development, and significance. *Science*, 223(4631), 22–27. <https://doi.org/10.1126/science.223.4631.22>
- Oviatt, C. A., Rudnick, D. T., Keller, A. A., Sampou, P. A., & Almqvist, G. T. (1986). A comparison of system ( $O_2$  and  $CO_2$ ) and C-14 measurements of metabolism in estuarine mesocosms. *Marine Ecology Progress Series*, 28, 57–67. <https://doi.org/10.3354/meps028057>
- Paerl, H. W., Rossignol, K. L., Hall, S. N., Peierls, B. L., & Wetz, M. S. (2010). Phytoplankton community indicators of short-and long-term ecological change in the anthropogenically and climatically impacted Neuse River Estuary, North Carolina, USA. *Estuaries and Coasts*, 33(2), 485–497. <https://doi.org/10.1007/s12237-009-9137-0>
- Reed, D. C., & Harrison, J. A. (2016). Linking nutrient loading and oxygen in the Coastal Ocean: A new global scale model. *Global Biogeochemical Cycles*, 30(3), 447–459. <https://doi.org/10.1002/2015gb005303>
- Reynolds-Fleming, J. V., Fleming, J. G., & Luettich, R. A. (2002). Portable autonomous vertical profiler for estuarine applications. *Estuaries*, 25(1), 142–147. <https://doi.org/10.1007/BF02696058>
- Reynolds-Fleming, J. V., & Luettich, R. A. (2004). Wind-driven lateral variability in a partially mixed estuary. *Estuarine, Coastal and Shelf Science*, 60(3), 395–407. <https://doi.org/10.1016/j.ecss.2004.02.003>
- Riemann, B., Carstensen, J., Dahl, K., Fossing, H., Hansen, J. W., Jakobsen, H. H., et al. (2015). Recovery of Danish coastal ecosystems after reductions in nutrient loading: A holistic ecosystem approach. *Estuaries and Coasts*, 39(1), 82–97. <https://doi.org/10.1007/s12237-015-9980-0>
- Rizzo, W. M., & Christian, R. R. (1996). Significance of subtidal sediments to heterotrophically-mediated oxygen and nutrient dynamics in a temperate estuary. *Estuaries*, 19(2), 475–487. <https://doi.org/10.2307/1352464>
- Schumann, U., & Gerz, T. (1995). Turbulent mixing in stably stratified shear flows. *Journal of Applied Meteorology and Climatology*, 34(1), 33–48. <https://doi.org/10.1175/1520-0450-34.1.33>
- Scully, M. E. (2010a). The importance of climate variability to wind-driven modulation of hypoxia in Chesapeake Bay. *Journal of Physical Oceanography*, 40(6), 1435–1440. <https://doi.org/10.1175/2010jpo4321.1>
- Scully, M. E. (2010b). Wind modulation of dissolved oxygen in Chesapeake Bay. *Estuaries and Coasts*, 33(5), 1164–1175. <https://doi.org/10.1007/s12237-010-9319-9>
- Scully, M. E. (2013). Physical controls on hypoxia in Chesapeake Bay: A numerical modeling study. *Journal of Geophysical Research: Oceans*, 118(3), 1239–1256. <https://doi.org/10.1002/jgrc.20138>
- Scully, M. E., Friedrichs, C., & Brubaker, J. (2005). Control of estuarine stratification and mixing by wind-induced straining of the estuarine density field. *Estuaries*, 28(3), 321–326. <https://doi.org/10.1007/BF02693915>
- Simpson, J. H., & Bowers, D. (1981). Models of stratification and frontal movement in shelf seas. *Deep-Sea Research, Part A: Oceanographic Research Papers*, 28(7), 727–738. [https://doi.org/10.1016/0198-0149\(81\)90132-1](https://doi.org/10.1016/0198-0149(81)90132-1)
- Simpson, J. H., Sharples, J., & Rippeth, T. P. (1991). A prescriptive model of stratification induced by freshwater runoff. *Estuarine, Coastal and Shelf Science*, 33(1), 23–35. [https://doi.org/10.1016/0272-7714\(91\)90068-M](https://doi.org/10.1016/0272-7714(91)90068-M)
- Smith, L. M., Silver, C. M., & Oviatt, C. A. (2012). Quantifying variation in water column photosynthetic quotient with changing field conditions in Narragansett Bay, RI, USA. *Journal of Plankton Research*, 34(5), 437–442. <https://doi.org/10.1093/plankt/fbs011>
- Trowbridge, J. H. (1992). A simple description of the deepening and structure of a stably stratified flow driven by a surface stress. *Journal of Geophysical Research*, 97(C10), 15529–15543. <https://doi.org/10.1029/92JC01512>
- Umlauf, L., Burchard, H., & Bolding, K. (2005). GOTM sourcecode and test case documentation, Devel version-pre, 4.
- Wanninkhof, R., Asher, W. E., Ho, D. T., Sweeney, C., & McGillis, W. R. (2009). Advances in quantifying air-sea gas exchange and environmental forcing. *Annual Review of Marine Science*, 1, 213–244. <https://doi.org/10.1146/annurev.marine.010908.163742>
- Whipple, A. C., Luettich, R. A., & Seim, H. E. (2006). Measurements of Reynolds stress in a wind-driven lagoonal estuary. *Ocean Dynamics*, 56(3–4), 169–185. <https://doi.org/10.1007/s10236-005-0038-x>
- Xie, X., & Li, M. (2018). Effects of wind straining on estuarine stratification: A combined observational and modeling study. *Journal of Geophysical Research: Oceans*, 123(4), 2363–2380. <https://doi.org/10.1002/2017jc013470>